UCLA
UCLA Electronic Theses and Dissertations

Title

Nonlinear time-delay dynamical model of oscillatory gene expression in BMP-4/9 vascular endothelial cell network

Permalink

https://escholarship.org/uc/item/40r7p5z0

Author

Yazdi, Daniel

Publication Date

2014

Peer reviewed|Thesis/dissertation

eScholarship.org Powered by the California Digital Library
University of California

UNIVERSITY OF CALIFORNIA

Los Angeles

Nonlinear Time-Delay Dynamical Model of Oscillatory Gene Expression in BMP-4/9 Vascular Endothelial Cell Network

A thesis submitted in partial satisfaction

of the requirements for the degree

Master of Science in Biomathematics

by

Daniel Yazdi

2014

© Copyright by

Daniel Yazdi

2014

ABSTRACT OF THE THESIS

Nonlinear Time-Delay Dynamical Model of Oscillatory Gene Expression in BMP-4/9 Vascular Endothelial Cell Network

by

Daniel Yazdi

Master of Science in Biomathematics

University of California, Los Angeles, 2014

Professor Alan Garfinkel, Co-chair

Professor Elliot Landaw, Co-chair

Bone morphogenic proteins (BMPs) and their inhibitors are increasingly being appreciated for their role in vascular development. Matrix Gla protein (MGP) and crosssveinless 2 (CV2) antagonize BMP-4 and BMP-9, respectively, and the expression of both are stimulated by time-delayed BMP-9/ALK1 signaling, while ALK1 is stimulated by delayed BMP-4 signaling. This double negative feedback system is an important regulator of endothelial cell differentiation, angiogenesis, and maturation. Our collaborators recently discovered oscillatory gene expression of these proteins in human pulmonary artery endothelial cells (HPAECs) undergoing maturation in cell culture. We set out to explore the biological mechanisms guiding this periodic gene expression and to propose a functional role for these oscillations. We used delay differential equations to mathematically model this network and applied dimensionless analysis to study the impact of relative protein degradation rates on oscillations. Monte Carlo parameter sampling and Hopf bifurcation analysis, while adjusting 1 and 2 parameters, helped identify conditions yielding periodic dynamics. We discovered that the presence of the activator, BMP-4, is critical for oscillations and that its inhibitor, MGP, opposes them, making their mutual regulation important for oscillatory gene expression. We

also identified other mechanisms for oscillations including the necessary existence of three time-delays, the presence of BMP-9 as a feedback regulator, and the function of CV2 as an indirect inhibitor of MGP. Findings from the cell culture experiments and the mathematical model led us to postulate that oscillations in this network are important for the maintenance of progenitor HPAECs and the lack of oscillations is associated with HPAEC maturation.

The thesis of Daniel Yazdi is approved.

Van Savage

Elliot Landaw, Committee Co-chair

Alan Garfinkel, Committee Co-chair

University of California, Los Angeles

2014

To my mother and father, Alfreda and Abraham Yazdi . . .

who—among so many other things—

always encouraged me to pursue my aspirations

while not being afraid to create a new path.

I would also like to dedicate this to my sister, Rebecca,

and other members of my family

for their love and support.

TABLE OF CONTENTS

0.1 Introduction 1

0.1.1 Presence of Oscillations in Biology 1

0.1.2 Mechanisms of Oscillations in Biology 2

0.1.3 Function of Oscillations in Biology 3

0.1.4 The BMP-4/9 network in endothelial cells 7

0.1.5 BMP, MGP, CV2 regulatory network 8

0.2 Methods 13

0.2.1 The Mathematical Model 13

0.2.2 Non-dimensionalization 15

0.2.3 Parameter Estimations 17

0.2.4 Monte Carlo Parameter Sampling for Oscillations 18

0.2.5 Hopf Bifurcation Analysis of Delay-Differential Equations . . . 21

0.2.6 Cell Culture Experiments 24

0.3 Results 25

0.3.1 Monte Carlo Simulation 25

0.3.2 1-Parameter Hopf Bifurcation Analysis 30

0.3.3 2-Parameter Hopf Bifurcation Analysis 45

0.4 Experimental Results 49

0.5 Discussion 55

References **60**

LIST OF FIGURES

0.1 **Root patterning in the Arabidopsis thaliana plant**: A). Oscillatory gene expression at the root tip establishes prebranch sites for new lateral root formation. B) The prebranch site subsequently grows new lateral roots. [1] 4

0.2 **Oscillations in Hes1 and Ngn2 gene expression**: A) Neuronal progenitor cells display oscillatory gene expression of Hes1, Dll1, and Ngn2. Differentiated neuronal cells bifurcate to sustained high and low levels of Ngn2, and Hes1 and Dll1, respectively. [2] 6

0.3 **Dynamical systems approach to cell differentiation**: A) Waddington epigenetic landscape with grooves representing genetic pathways to a more differentiated cell state, symbolized by local minima in the valleys [3]. B) Gene expression state space depiction of stem cells existing in an oscillatory attractor and differentiated cells gravitating to stable nodes [4] 7

0.4 **ALK1 mRNA expression**: 50 ng/ml of BMP-4 is added to cell culture at day 0. There is noticeable oscillatory gene expression of ALK1 in progenitor HPAECs. 8

0.5 **From stripes to spots**: A) In vitro patterns in cultured vascular mesenchymal cells and the numerical solution of the mathematical model. B) Treatment with exogenous inhibitor MGP (40 ng/ml) resulted in cell aggregation to a spot-like pattern instead of stripes. The spot pattern is replicated in the mathematical model by increasing the source term for MPG [5]. 10

0.6 **BMP Network Diagram**: Network diagram for biological relationship accounted for in the model. BMP-9 endogenous ligands bind to ALK1 receptor to stimulate production of CV2 and MGP with a transcriptional time delay of 20 and 6 hours respectively. CV2 and MGP bind and inhibit BMP-9 and BMP-4, respectively. BMP-4 autocatalytically produces itself through ALK2 signaling and activates ALK1 transcription with a time delay of 8 hours. BMP-4/ALK2 signaling is associated with EC progenitor state, while BMP9/ALK1signaling stimulates EC maturation. 12

0.7 **MC sampling parameter distributions**: the log parameter distributions that result in an oscillatory model output. A) γ_1, B) γ_2, C) γ_3, D) γ_4. 26

0.8 **Time-delay probability density functions**: the normal distributions are defined with a mean equal to the peak time delay, τ_n and a standard deviation equal to 10% τ_n. These distributions are used for MC sampling. 28

0.9 **Time-delay probability density functions**: the normal distributions are defined with a mean equal to the peak time delay, τ_n and a standard deviation equal to 10% τ_n. These distributions are used for MC sampling. 29

0.10 **BMP-4 degradation rate (γ_2) equilibrium point stability diagram** : The x-axis contains the parameter value and the y-axis represents the equilibrium points of the non-dimensional variables A= BMP-9, B= BMP-4, M=MGP, C = CV2. Red and blue dots symbolize stable and unstable equilibrium points, respectively. The green lines mark the boundary of the parameter regime exhibiting limit cycle dynamics. . . . 31

0.11 **BMP-4 degradation rate (γ_2) eigenvalue analysis for the equilibrium point exhibiting a Hopf bifurcation**: A) The eigenvalues of the transcendental characteristic equation after the Hopf bifurcation ($log_{10}(\gamma_2) = -1.6$). The rightmost complex conjugate eigenvalue has a positive real part indicating an unstable spiral equilibrium point. B) The real component of the eigenvalue for the equilibrium point undergoing the Hopf bifurcation as γ_2 is changed. This is the same eigenvalue for variables A, B, M, C, and S. There is a supercritical Hopf bifurcation (marked by green lines) and an equilibrium point annihilation. 33

0.12 **Limit cycle in time series**: A) The spiraling stable dynamics of the model before the Hopf bifurcation ($log_{10}(\gamma_2) = -1.65$). B) The limit cycle dynamics of the model after the Hopf bifurcation ($log_{10}(\gamma_2) = -1.6$). A = BMP-9, B = BMP-4, M=MGP, C=CV2, S=ALK1. 34

0.13 **BMP-9 degradation rate (γ_1) equilibrium point stability diagram** : The x-axis contains the parameter value and the y-axis represents the equilibrium points of the non-dimensional variables A= BMP-9, B= BMP-4, M=MGP, C = CV2. Red and blue dots symbolize stable and unstable equilibrium points, respectively. The green lines mark the boundary of the parameter regime exhibiting limit cycle dynamics. . . . 36

0.14 **BMP-9 degradation rate (γ_1) eigenvalue analysis for the equilibrium point exhibiting a Hopf Bifurcation**: The real component of the eigenvalue for the equilibrium point undergoing the Hopf bifurcation as γ_1 is changed. This is the same eigenvalue for variables A, B, M, C, and S. There is a supercritical Hopf bifurcation and an equilibrium point annihilation. 37

0.15 **MGP degradation rate (γ_3) equilibrium point stability diagram** : The x-axis contains the parameter value and the y-axis represents the equilibrium points of the non-dimensional variables A= BMP-9, B= BMP-4, M=MGP, C = CV2. Red and blue dots symbolize stable and unstable equilibrium points, respectively. The green lines mark the boundary of the parameter regime exhibiting limit cycle dynamics. . . . 38

0.16 **MGP degradation rate (γ_3) eigenvalue analysis for the equilibrium point exhibiting a Hopf Bifurcation**: The real component of the eigenvalue for the equilibrium point undergoing the Hopf bifurcation as γ_3 is changed. This is the same eigenvalue for variables A, B, M, C, and S. There is a supercritical Hopf bifurcation and an equilibrium point annihilation. 39

0.17 **CV2 degradation rate (γ_4) equilibrium point stability diagram** : The x-axis contains the parameter value and the y-axis represents the equilibrium points of the non-dimensional variables A= BMP-9, B= BMP-4, M=MGP, C = CV2. Red and blue dots symbolize stable and unstable equilibrium points, respectively. The green lines mark the boundary of the parameter regime exhibiting limit cycle dynamics. . . . 40

0.18 **CV2 degradation rate (γ_4) eigenvalue analysis for the equilibrium point exhibiting a Hopf Bifurcation**: The real component of the eigenvalue for the equilibrium point undergoing the Hopf bifurcation as γ_4 is changed. This is the same eigenvalue for variables A, B, M, C, and S. There are two Hopf bifurcations. 41

0.19 **τ_1 eigenvalue analysis for the equilibrium point undergoing a Hopf bifurcation**: The real component of the eigenvalue for the equilibrium point undergoing the Hopf bifurcation as $\hat{\tau_1}$ is changed. This is the same eigenvalue for variables A, B, M, C, and S. $Re(\lambda) > 0$ corresponds to periodic dynamics. 42

0.20 τ_2 **eigenvalue analysis for the equilibrium point undergoing a Hopf bifurcation**: The real component of the eigenvalue for the equilibrium point undergoing the Hopf bifurcation as $\hat{\tau_2}$ is changed. This is the same eigenvalue for variables A, B, M, C, and S. $Re(\lambda) > 0$ corresponds to periodic dynamics. 43

0.21 τ_3 **eigenvalue analysis for the equilibrium point undergoing a Hopf bifurcation**: The real component of the eigenvalue for the equilibrium point undergoing the Hopf bifurcation as $\hat{\tau_3}$ is changed. This is the same eigenvalue for variables A, B, M, C, and S. $Re(\lambda) > 0$ corresponds to periodic dynamics. 44

0.22 **BMP-4 and BMP-9 degradation rate (γ_2, γ_1) stability analysis on the equilibrium point exhibiting a Hopf bifurcation**: γ_1 and γ_2 parameter space analysis for limit cycles. These eigenvalues are the same for the variables A, B, M, C, and S. The red dot marks locations with stable dynamics. The blue dot marks unstable spiral nodes that result in oscillatory kinetics. 46

0.23 **BMP-4 and MGP degradation rate (γ_2, γ_3) stability analysis for the equilibrium point exhibiting a Hopf bifurcation**: γ_1 and γ_3 parameter space analysis for limit cycles. These eigenvalues are the same for the variables A, B, M, C, and S. The red dot marks locations with stable dynamics. The blue dot marks unstable spiral nodes that result in oscillatory kinetics. 47

0.24 **BMP-4 and CV2 degradation rate (γ_2, γ_4) stability analysis for the equilibrium point exhibiting a Hopf bifurcation**: γ_1 and γ_4 parameter space analysis for limit cycles. These eigenvalues are the same for the variables A, B, M, C, and S. The red dot marks locations with stable dynamics. The blue dot marks unstable spiral nodes that result in oscillatory kinetics. 48

0.25 **ALK1 relative mRNA expression**: fold change of ALK1 expression after the addition of either BMP-4 (50 ng/ml), BMP-9 (10 ng/ml), Control, or Noggin (100 ng/ml) & anti-BMP-9 (ng/ml) to HPAEC culture. The vertical line marks the approximate point of confluence. 50

0.26 **CV2 relative mRNA expression**: fold change of CV2 expression after the addition of either BMP-4 (50 ng/ml), BMP-9 (10 ng/ml), Control, or Noggin (100 ng/ml) & anti-BMP-9 (ng/ml) to HPAEC culture. The vertical line marks the approximate point of confluence. 51

0.27 **MGP relative mRNA expression**: fold change of CV2 expression after the addition of either BMP-4 (50 ng/ml), BMP-9 (10 ng/ml), Control, or Noggin (100 ng/ml) & anti-BMP-9 (ng/ml) to HPAEC culture. The vertical line marks the approximate point of confluence. 52

0.28 **CD34 relative mRNA expression**: fold change of CV2 expression after the addition of either BMP-4 (50 ng/ml), BMP-9 (10 ng/ml), Control, or Noggin (100 ng/ml) & anti-BMP-9 (ng/ml) to HPAEC culture. The vertical line marks the approximate point of confluence. 53

LIST OF TABLES

0.1 **Model Parameters**: This table contains the approximate values, units, and the biological functions of the dimensional and dimensionless parameters used in this study. 19

0.2 **MC sampling parameter distribution statistics with fixed delays**: the median values, median 95% C.I., and the range for each parameter distribution. 27

0.3 **MC sampling parameter distribution statistics with a normally distributed delays**: the median values, median 95% C.I., and the range for each parameter distribution. The time-delays are randomly sampled from normal distributions centered around τ_n. 29

0.4 **1-Parameter Hopf bifurcation analysis of limit cycle regimes**: the parameter values for which the model exhibits limit cycle dynamics while adjusting the indicated parameter and keeping the rest fixed. . . . 44

ACKNOWLEDGMENTS

I would like to acknowledge Dr. Alan Garfinkel for captivating my interest in nonlinear dynamics and for being an incredible mentor. I would also like to thank our experimental collaborators Dr. Kristina Bostrom and Dr. Pierre Guihard, for whom without, this project would not have been possible. Finally, I would like to thank Mr. West and Dr. Feynman for continually inspiring me to approach the world with naiveté of a child and the rigor of a scientist.

0.1 Introduction

0.1.1 Presence of Oscillations in Biology

Crafted by evolution, biological systems are highly regulated to perform their designated function in a robust, reliable manner. This often involves the necessary checks and balances in the form of feed-forward and feedback regulation guided by complex nonlinear dynamics. However, traditional approaches in understanding biological systems tend to view physiology from a homeostatic perspective, with the body responding to internal and external perturbations to restore steady-state equilibrium. This approach is incorrect as many variables in the body have oscillatory behaviors including temperature, blood pressure, hormone concentrations, and cardiac cycles that occur at various time scales [6, 7, 8]. Temperature regulation is often misinterpreted as maintenance of a hypothalamic set point amid internal and external temperature fluctuations, when instead body temperature naturally exhibits endogenously generated oscillations with a period of approximately one day [7]. Clinical studies have also demonstrated self-sustained high amplitude oscillations in human insulin and glucose concentrations, countering the notion of their set homeostatic concentrations [9, 10].

In addition to being a normal component of physiological processes, oscillations can contribute to the pathophysiology of certain diseases. Patients with several neurological conditions including Parkinson's disease and essential tremor display motor oscillations at signature frequencies. The origins of these oscillations are multifactorial in nature with contributions from central nervous system oscillations, motor unit firing properties, and reflex loop resonances that play a role in feedback regulation of motor control [11]. In cardiac fibrillation, oscillations in cardiac wavelength, the product of action potential duration and conduction velocity, cause reentrant waves of excitation to enter spatiotemporal chaos, the substrate of fibrillation. [12]. These are just a subset of the many examples of important oscillatory dynamics in physiology to display their significance in health and disease.

0.1.2 Mechanisms of Oscillations in Biology

The prevalence of oscillations in biological systems begs for an understanding of the mechanisms guiding their behavior. With this knowledge, it is possible to mathematically and computationally model the system to recreate the experimental findings and to hypothesize how perturbations will affect the dynamics of the system. Mechanistically, there are two important factors inherent in the creation of oscillations: steep negative feedback and time delays. Negative feedback occurs when the product of a process inhibits its own creation, a form of self-regulation. With appropriate feedback strength, this process can exist in a stable state. However, when the feedback gain crosses a critical value, it can push the system to a state of instability that contains oscillatory dynamics. This type of self-regulation is ubiquitous in biological processes, including the p53 pathway in cell cycle regulation, as a mechanism to counter the unpredictable perturbations present in the internal and external environment [13].

Time-delays, the duration necessary for a signal to act on its target, are another key-ingredient for the creation of oscillations. Regardless of the system, there is always a finite time-delay for any signal that inherently makes the system more prone to incur oscillatory dynamics. A few examples in the biological realm include transcriptional and translational delays associated with gene expression and protein synthesis, the passage of hormones through the circulatory system to reach effector glands, and cell signaling cascades through G-coupled protein receptors [14, 15, 16]. If the delay is appreciable relative to the time scale of other processes in the system, the time-delay can be mathematically modeled by replacing intermediate signaling events with finite time-delays between the variables of interest. Doing so reduces the number of variables and parameters in the mathematical model in an effort to simplify its analysis, but at the cost of being less reflective of reality.

0.1.3 Function of Oscillations in Biology

0.1.3.1 Temporal Compartmentalization

The ubiquitous presence of oscillations in nature is correlated with a functional advantage of having such a behavior. Periodic dynamics allow ”temporal compartmentalization” of competing forces [17]. The metabolic breakdown of glucose in glycolysis depends on the activity of enzymes such as phosphofructokinase, and 1,6-biphosphatase, for the ultimate creation of ATP. Gluconeogenesis, the endergonic reversal of glycolysis, produces glucose when additional amounts are needed. Interestingly, glycolysis requires the enzymatic rate of phosphofructokinase to be much greater than that of 1,6-biphosphatase, while gluconeogenesis demands the opposite. The cell mediates the coexistence of the exclusive conditions through anti-phase oscillations of the two enzymes, allowing each process to occur while the other is not [18].

0.1.3.2 Spatial Structure

In addition to temporal compartmentalization, oscillations have the ability to produce spatial structure. A classical example of this is somite formation in a developing embryo. A somite is a precursor for a segment of vertebrae body axis that develops into ribs, muscles, peripheral nerves, and blood vessels. Growth occurs along the anterior-posterior axis with progression in the posterior direction. This segmentation clock process has a traveling wavefront of oscillating genes in the presomitic mesoderm that creates new somites posterior to the previous one with each period of the cycle [19]. Experimental studies demonstrate oscillatory expression of genes in Notch signaling with a period of 90 minutes in chick embryo [20]. Microarray transcriptome analysis has shown that genes comprising the segmentation clock possess anti-phase oscillations between members of the antagonistic Notch/FGF and Wnt pathways [21]. This demonstrates the importance of inhibitory feedback regulation in the creation of oscillations and the functional role of oscillations in somitogenesis.

Analogous to a developing embryo, lateral root branching in plants follows a similar pattern of oscillatory gene expression along a traveling shoot. This process converts temporal information into periodic spatial patterning. Expression of the DR5 marker gene oscillates in the Arabidopsis root tip, known as the oscillation zone (OZ) [22]. The cycling genes mark the locations for lateral roots at the pre-branch sites as the root axis elongates (Figure 0.1). Microarray analysis of genes in the OZ revealed around 2000 genes oscillating in phase with DR5, 1,400 cycling out of phase, and no genes in other phases, similar to findings in the segmentation clock of vertebrates [22]. Somitogenesis and lateral root branching demonstrate an evolutionary convergent solution for creating spatially repeating structures from autonomous cyclic gene expression.

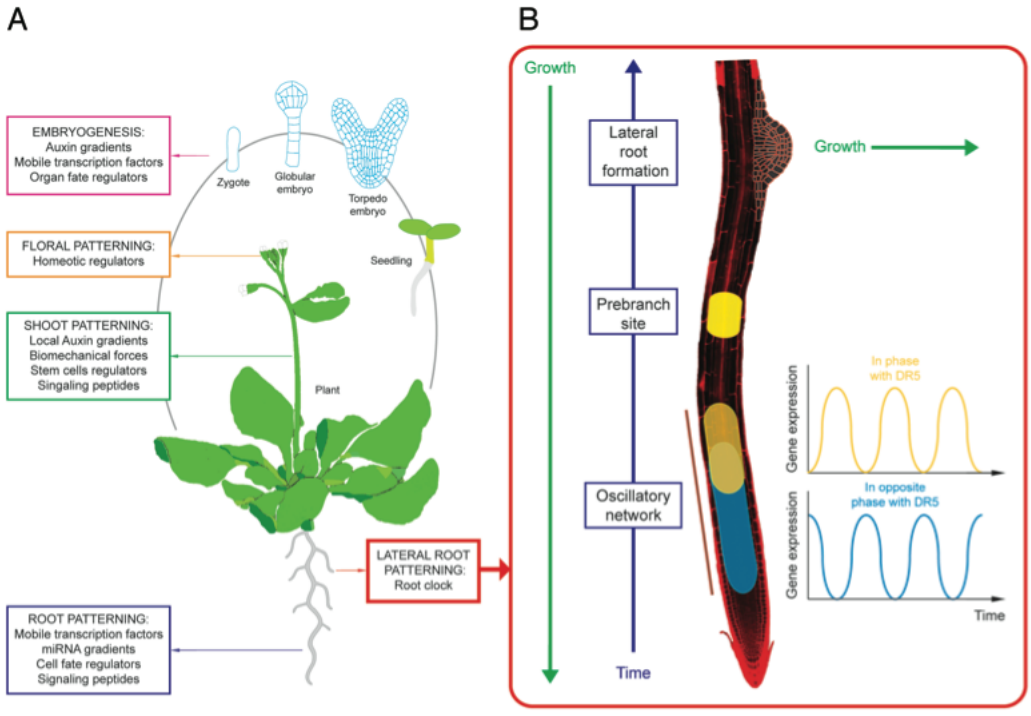


Figure 0.1: **Root patterning in the Arabidopsis thaliana plant**: A). Oscillatory gene expression at the root tip establishes prebranch sites for new lateral root formation. B) The prebranch site subsequently grows new lateral roots. [1]

0.1.3.3 Cell Differentiation

Oscillatory gene expression has recently been implicated in maintaining the progenitor status of various cell types. In neural progenitor cells, Notch signaling activates downstream expression of the basic helix-loop-helix transcriptional repressor, Hes1, which inhibits transcription of proneural genes [2]. Inactivation of Hes1 has the opposite effect of upregulating expression of proneural genes. It has been shown that Hes1 gene expression autonomously oscillates in dividing neural progenitor cells with a period of 2-3 hours via negative feedback on its own promoter [23]. Furthermore, the expression of the proneural gene Neurogenin-2 (Ngn2) also oscillates in neural progenitor cells under the regulation of Hes1. As the progenitor cells undergo neuronal differentiation, the system transitions from oscillating gene expression to sustained low and high levels of Hes1 and Ngn2, respectively (Figure 0.2). Maintained elevated expression of Ngn2 is believed to be necessary for neuronal differentiation because its downstream differentiation genes have a delayed response to Ngn2 signaling [2]. Thus, negative feedback and time-delays are important mechanisms underlying the oscillatory gene expression critical for progenitor cell maintenance, while the lack of periodic behavior is associated with neuronal differentiation.

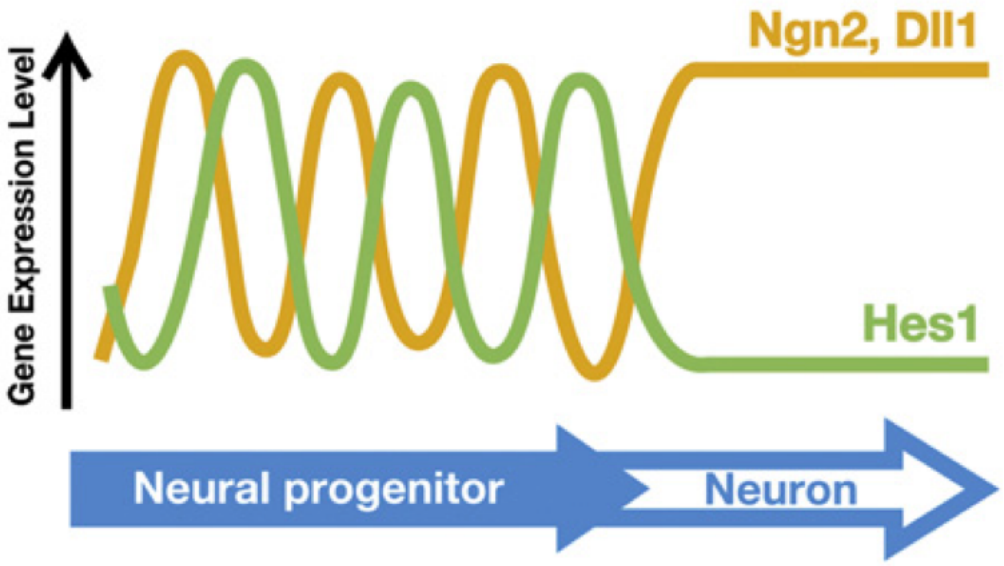


Figure 0.2: **Oscillations in Hes1 and Ngn2 gene expression**: A) Neuronal progenitor cells display oscillatory gene expression of Hes1, Dll1, and Ngn2. Differentiated neuronal cells bifurcate to sustained high and low levels of Ngn2, and Hes1 and Dll1, respectively. [2]

This concept of oscillatory dynamics in stem and progenitor cells introduces the idea of cell types belonging to different dynamical attractors in gene expression state space. In 1942, Waddington proposed the idea of an epigenetic landscape where cells metaphorically traverse grooves on the slopes to rest at local minimum representing a specific cell fate (Figure 0.3). This metaphor can be extended to a dynamical systems viewpoint of cell differentiation with unique gene signatures comprising stable state space attractors. Perturbations to this system, such as inhibition of Hes1 gene expression, create a bifurcation in the system pushing the cell to a more differentiated attractor.

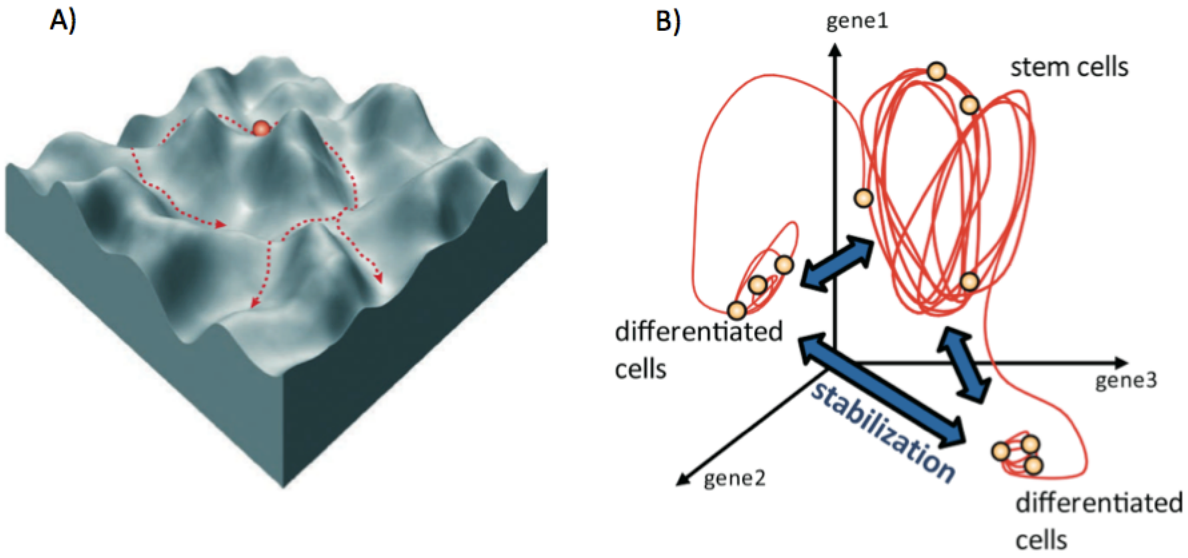


Figure 0.3: **Dynamical systems approach to cell differentiation**: A) Waddington epigenetic landscape with grooves representing genetic pathways to a more differentiated cell state, symbolized by local minima in the valleys [3]. B) Gene expression state space depiction of stem cells existing in an oscillatory attractor and differentiated cells gravitating to stable nodes [4]

.

0.1.4 The BMP-4/9 network in endothelial cells

The emergence of oscillatory gene expression patterns as an important factor in cell differentiation motivated us to mathematically study the bone morphogenic protein 4 (BMP-4) and BMP-9 regulatory network in vascular endothelial cells. Our collaborators in the Bostrom Lab at UCLA identified the oscillatory expression of several genes in this network in progenitor human pulmonary vascular endothelial cells (HPAECs) that transitioned to non-oscillatory sustained expression upon differentiation (Figure 0.4).

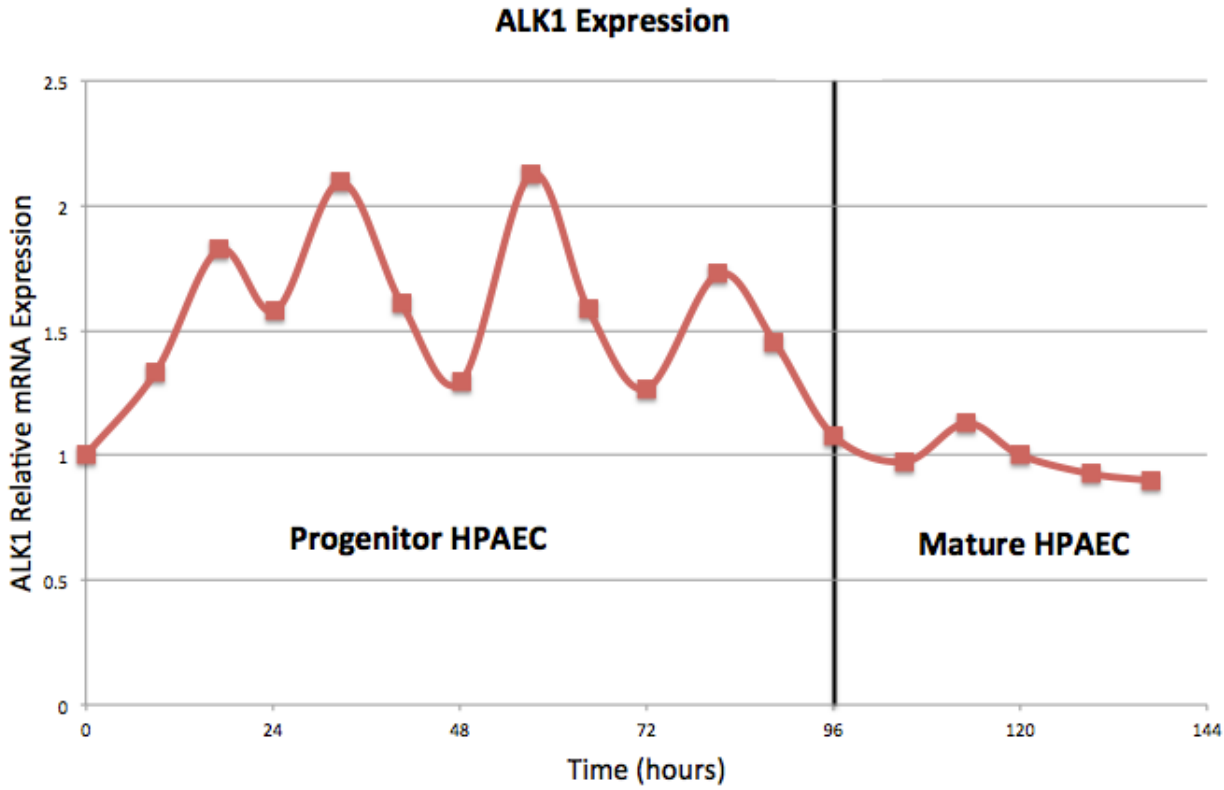


Figure 0.4: **ALK1 mRNA expression**: 50 ng/ml of BMP-4 is added to cell culture at day 0. There is noticeable oscillatory gene expression of ALK1 in progenitor HPAECs.

0.1.5 BMP, MGP, CV2 regulatory network

Vascular development is an integral component of embryogenesis, organogenesis, and wound healing, with BMP-4 and BMP-9 recently emerging as important proteins in these processes [24, 25]. BMPs are part of the TGFβ superfamily and act as morphogens guiding the developmental architecture of various parts of the body throughout life. BMP-4 is an essential stimulator of differentiation of human embryonic stem cells to vascular progenitor cells through Smad signaling and is responsible for inducing angiogenesis [26, 24] . Opposing the actions of BMP-4, BMP-9 inhibits VEGF-induced angiogenesis and bFGF-induced endothelial cell (EC) proliferation [27]. They

are connected to each other through the activin-receptor like kinase 1 (ALK1), where BMP-4 induces ALK1 expression and BMP-9 binds to ALK1 as a ligand for downstream signaling [28]. Furthermore, mutations in ALK1 are associated with hemorrhagic telangiectasia (HHT) which manifests itself through ateriovenous malformations (AVMs) [29].

The BMP signaling network is regulated in part by proteins that operate in a coupled negative feedback manner. Matrix GLA protein (MGP) and crossveinless 2 (CV2) bind directly to BMP, and inhibit its activity [30]. MGP is induced by BMP-9/ALK1 signaling and inhibits the activity of BMP-2, BMP-4, and BMP-7. Through BMP-4 inhibition, MGP antagonizes angiogenesis, and the lack of MGP results in AVMs similar those seen with reduced ALK1 levels [31]. CV2 expression is also induced by BMP-9/ALK1 signaling and operates in a negative feedback regulatory manner by preferentially binding to and inhibiting BMP-9, thereby reducing BMP-9/ALK1 signaling [32]. CV2 is known to antagonize EC differentiation with the mechanism believed to be through its inhibition of BMP-9. Experimental evidence indicates that mice without CV2 display abnormal BMP signaling with increased vascular endothelium thickness and increased expression of EC differentiation markers [32].

Previous mathematical analyses of BMP, in this context, have concentrated on the activation-inhibition dynamics between BMP-2 and MGP. Garfinkel et al. studied a reaction-diffusion partial differential equation, modeling mesenchymal stem cell organization [5]. The mathematical model predicted spatial pattern formation in the form of stripes, spots, and stripe-doubling, and was replicated in an in-vitro vascular mesenchymal cell culture (Figure 0.5). This is clinically important because ectopic bone organizes in nodular patterns within cardiac valves in adult diseases such as atherosclerosis and calcific valvular stenosis. This model provides a glimpse of the mechanism governing the pathophysiology of such diseases. Adjusting parameters in the model to resolve the disease phenotype can also help identify potential therapies.

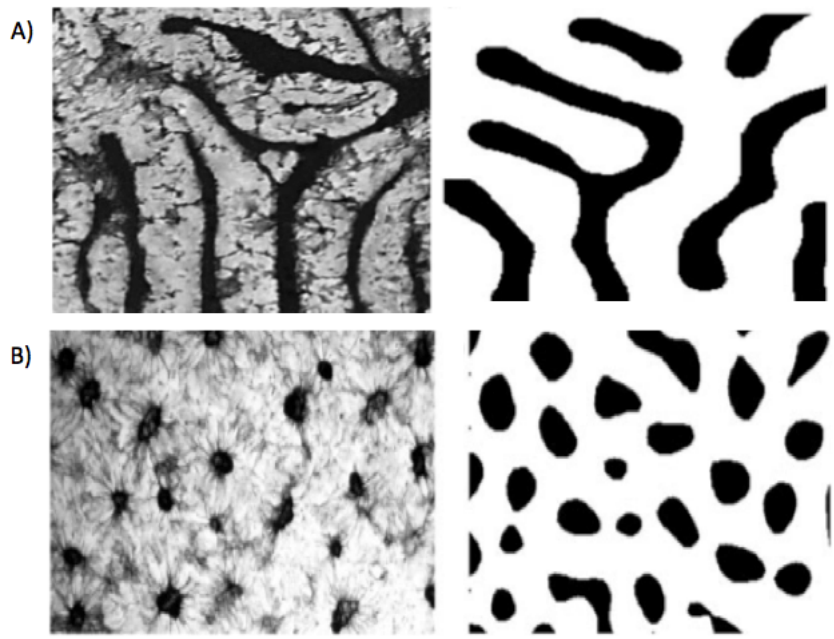


Figure 0.5: **From stripes to spots**: A) In vitro patterns in cultured vascular mesenchymal cells and the numerical solution of the mathematical model. B) Treatment with exogenous inhibitor MGP (40 ng/ml) resulted in cell aggregation to a spot-like pattern instead of stripes. The spot pattern is replicated in the mathematical model by increasing the source term for MPG [5].

The BMP, MGP dynamical system was further studied for Turing pattern formation in the context of pulmonary vascular development [33]. Increased levels of MGP in the transgenic mice acted antagonistically against BMP-4 and disrupted lung vascular patterning with reduced side branching. A computational model using similar reaction-diffusion partial differential equations recreated the reduced side branching with increased MGP concentrations, supporting the activator-inhibitor role of these morphogens in pulmonary vascular development. As highlighted by the previous examples, the BMP transcriptional system is active in numerous locations and times throughout development by acting on different downstream transcriptional binding domains responsible for regulating gene expression. As a result, this system can display various functional roles in a context dependent manner.

Previous work modeling the BMP regulatory network has focused on elucidat-

ing its spatiotemporal dynamics, especially in pattern formation [5, 33]. In the early modeling efforts the biological kinetics, the ODE part of the PDE, had only equilibrium dynamics, including bistability [5]. The role of temporal fluctuations in biological systems, such as compartmentalization, spatial structuring, and stem cell differentiation, all of which are connected to the BMP regulatory network, makes it of interest to study the capabilities of the system for oscillations. Specifically, we designed a mathematical model of the BMP network in vascular endothelial cells, guided by the molecular dynamics and time-delays of the system, to explore the conditions yielding oscillatory behavior. In conjunction with our experimental results, we hypothesize that the oscillatory dynamics in the system correspond to the maintenance of the EC progenitor state, while the elimination of oscillations is associated with differentiation into mature ECs. Furthermore, analyses of the parameters in the model indicate that the presence of BMP-4 induces oscillations, while too much of its antagonist, MGP, inhibits them.

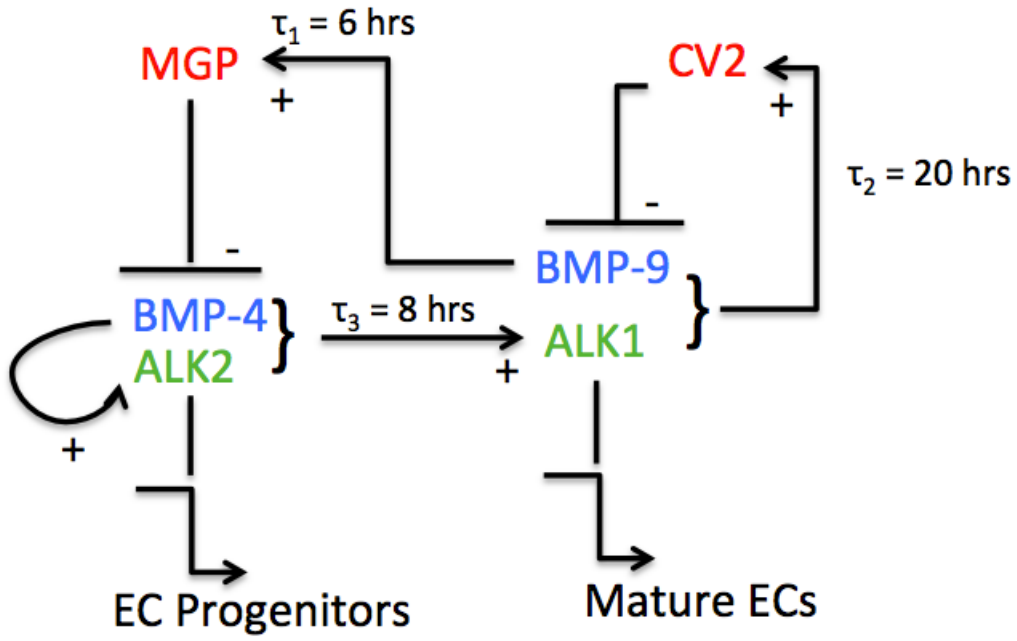


Figure 0.6: **BMP Network Diagram**: Network diagram for biological relationship accounted for in the model. BMP-9 endogenous ligands bind to ALK1 receptor to stimulate production of CV2 and MGP with a transcriptional time delay of 20 and 6 hours respectively. CV2 and MGP bind and inhibit BMP-9 and BMP-4, respectively. BMP-4 autocatalytically produces itself through ALK2 signaling and activates ALK1 transcription with a time delay of 8 hours. BMP-4/ALK2 signaling is associated with EC progenitor state, while BMP9/ALK1signaling stimulates EC maturation.

0.2 Methods

0.2.1 The Mathematical Model

We constructed a simplified mathematical model of the BMP-4/9 regulatory network. The model postulates 5 variables representing protein concentrations that are modeled with nonlinear time-delay differential equations. The equations model the rate of change in the molecule concentrations (ng/ml) over time (hr) and numerical integration in $Mathematica$ computes the concentrations as a function of time. The kinetic reaction terms are based on known molecular interactions of the five variables: BMP-4, BMP-9, MGP, CV2, and ALK1.

$$BMP9: \quad \frac{dA}{dt} = \frac{k_1}{\zeta C + \delta_1} - \mu_1 A \tag{0.1}$$

$$BMP4: \quad \frac{dB}{dt} = \frac{k_2 B^2}{(\alpha^2 + B^2)(\rho M + \delta_2)} - \mu_2 B \tag{0.2}$$

$$MGP: \quad \frac{dM}{dt} = k_3 A(t-\tau_1) S(t-\tau_1) - \mu_3 M \tag{0.3}$$

$$CV2: \quad \frac{dC}{dt} = k_4 A(t-\tau_2) S(t-\tau_2) - \mu_4 C \tag{0.4}$$

$$ALK1: \quad \frac{dS}{dt} = k_5 B(t-\tau_3)^2 - \mu_5 S \tag{0.5}$$

In Equation (0.1), the variable A is the concentration of BMP-9 (ng $\cdot$ ml). BMP-9 is a major circulating vascular quiescence factor produced by hepatocytes and intrahepatic biliary cells and is present in the human plasma at a concentration of 2-12 ng/ml [34]. The source term of BMP-9 is accounted for by a constant production rate of k_1. CV2 interrupts EC differentiation and preferentially inhibits BMP-9 by binding to it, acting as a negative feedback in BMP-9/ALK1 signaling [32]. The inhibitory interaction of CV2 with BMP-9 is modeled with the CV2 variable, C, in the denominator of the BMP-9 source term. The parameter ζ models the strength of CV2 inhibition on BMP-9. A larger ζ equates to a faster removal of BMP-9 from the system. In Equation

(0.1), the parameter δ_1 models the baseline inhibition of BMP9 without any CV2. Since there should not be inhibition of BMP-9 without CV2, $\delta_1 = 1$. BMP-9 is removed from the system by degradation at a rate proportional to its concentration, μ_1 (hr^{-1}).

Equation (0.2) describes the variable B, the concentration of BMP-4. Similar to some other members of the $TGF\beta$ superfamily such as BMP-2, BMP-4 is regulated by an autocatalytic loop [35]. The activation of BMP-4 is modeled by a sigmoidal function to capture its autocatalysis and the saturation dynamics when the concentration of BMP-4 is elevated. The parameter k_2 (ng $\cdot$ ml^{-1} $\cdot$ hr^{-1}) represents the maximum production rate of the BMP-4 autocatalytic loop, V_{max}. The parameter α is the concentration of BMP-4 when the reaction rate is half of V_max. Furthermore, MGP inhibits BMP-4 by directly binding to it, supporting the inhibitory MGP variable, M, in the denominator [33]. Analogous to Equation (0.1), the parameter ρ (ng$^{-1}\cdot$ ml) measures the inhibitory strength of MGP on BMP-4. The baseline inhibition parameter $\delta_2 = 1$ for the same reason $\delta_1 = 1$. BMP-4 is eliminated at the rate μ_2 (hr^{-1}).

The dynamics of the inhibitory molecule MGP are captured in Equation (0.3). MGP is produced as a downstream product of BMP-9/ALK1 signaling. Previous studies from the Bostrom Lab have shown that MGP expression peaked 6 hours after treatment of Human aortic endothelial cells (HAECs) with BMP-9 [32]. As a result there is an imbedded time delay, $\tau_1 = 6$ hrs. The BMP-9/ALK1 ligand-substrate interaction is modeled by the product of the two concentrations with a production rate, k_3 (ng$^{-1}\cdot$ ml $\cdot$ hr^{-1}). MGP is eliminated with a rate of μ_3 (hr^{-1}).

CV2 is another inhibitory molecule in this system represented by variable C and modeled by Equation (0.4). Similar to MGP, CV2 production is downstream BMP-9/ALK1 signaling. Expression of MGP precedes that of CV2 with a peak expression occurring 20 hours after HAEC treatment with BMP-9 [32].The time delay from BMP-9/ALK1 is captured by parameter $\tau_2 = 20$ hrs. The production of CV2 is modeled by the product of BMP-9 and ALK1 concentration with a rate of k_4 (ng$^{-1}\cdot$ ml $\cdot$ hr^{-1}). CV2 is eliminated with a degradation rate of μ_4 (hr^{-1}).

ALK1, the preferred membrane bound receptor for BMP-9, is modeled by Equation (0.5) [27]. BMP-4 signaling is the driving factor for ALK1 expression [25]. ALK1 expression peaks 8 hours after treating HAECs with BMP-4, making $\tau_3 = 8$ hrs [32]. Parameter k_5 (hr^{-1}) represents the production rate of ALK1 from BMP-4 signaling. ALK1 elimination occurs primarily through endocytosis from the plasma membrane. Experimental studies have demonstrated that this rate is approximately 1.5 hr^{-1}, which is the value assigned to μ_5 [36]. BMP turnover is thought to primarily occur through BMP-bound receptor endocytosis since no extracellular proteases targeting ligands of the TGFβ superfamily have been identified [30]. As a result, the degradation rates μ_1 and μ_2, for BMP9 and BMP4, respectively, should be within several orders of μ_5.

0.2.2 Non-dimensionalization

The dimensional model for this system contains 13 parameters when excluding the three time delays and baseline inhibition rates. Non-dimensionalization reduces the parameter dimensionality to 7 by lumping the parameters into dimensionless groups. It also simplifies the analysis of the system by transforming absolute parameter values into relative ratios. A sense of *size* is appreciated through relative comparisons of parameters values. The non-dimensional time $\hat{t}$ is set as the ratio of time t (hrs) and a time constant T, that we define to be $\frac{1}{\mu_5}$, the endocytosis rate of ALK1 [36]. Thus, the unitless parameter $\hat{t} = \frac{t}{T} = t \cdot \mu_5$, whose value can be thought of as the total number of ALK1 endocytoses occurring. Subsequent dimensional analysis yields the unitless parameters:

$$\theta_1 = \frac{\mu_5 \alpha^2}{k_2^2}, \quad \theta_2 = \frac{\rho \alpha^4 k_1 k_3 k_5}{\mu_5 k_2^2}, \quad \theta_3 = \frac{\zeta \alpha^4 k_1 k_4 k_5}{\mu_5 k_2^2},$$

$$\gamma_1 = \frac{\mu_1}{\mu_5}, \qquad \gamma_2 = \frac{\mu_2}{\mu_5}, \qquad \gamma_3 = \frac{\mu_3}{\mu_5}, \qquad \gamma_4 = \frac{\mu_4}{\mu_5}$$

This approach transforms the four degradation parameters, $\mu_1,\ \mu_2,\ \mu_3,\ \mu_4$, into ratios between BMP-9, BMP-4, MGP, and CV2 degradation rates and the endocytosis rate of ALK1, captured by the parameters $\gamma_1, \gamma_2, \gamma_3, \gamma_4$, respectively. The system dynamics can be studied in terms of relative degradation kinetics instead of absolute ones. The remaining 3 parameters θ_1, θ_2, and θ_3 are not as easily interpreted. Experimental data from our collaboration with the Bostrom Lab and parameters from the literature help provide approximations for these values.

Dimensional analysis also adjusts the model variables to ones lacking dimension. Generically, for dimensional a variable X, we define $X = X^*\bar{X}$, where $\bar{X}$ is the dimensionless variable and X^* is the transforming constant. From this we obtained

$$\begin{aligned} \bar{A} &= A\left(\frac{\mu_5}{k_1}\right), \quad \bar{B} = B\left(\frac{k_2}{\mu_5\alpha}\right), \quad \bar{M} = M\rho \\ \bar{C} &= C\zeta, \quad \bar{S} = S\left(\frac{k_2^2}{k_5\mu_5\alpha^2}\right). \end{aligned}$$

The variables $\bar{A}, \bar{B}, \bar{C}, \bar{M}$, and $\bar{S}$ are the dimensionless forms of A, B, C, M, and S respectively. In addition, we have dimensionless time-delay constants, $\hat{\tau_n}$, obtained by the relationship $\hat{\tau} = \tau \cdot \mu_5$. This yields our new time-delays

$$\hat{\tau_1} = 9, \quad \hat{\tau_2} = 30, \quad \hat{\tau_3} = 12$$

The resulting non-dimensional system of time-delay ordinary differential equa-

tions is:

$$BMP9: \quad \frac{d\bar{A}}{d\hat{t}} = \frac{1}{\bar{C}+1} - \gamma_1 \bar{A} \tag{0.6}$$

$$BMP4: \quad \frac{d\bar{B}}{d\hat{t}} = \frac{\bar{B}^2}{1+\bar{M}+\theta_1 \bar{B}^2(\bar{M}+1)} - \gamma_2 \bar{B} \tag{0.7}$$

$$MGP: \quad \frac{d\bar{M}}{d\hat{t}} = \theta_2 \bar{A}(\hat{t}-\hat{\tau_1})\bar{S}(\hat{t}-\hat{\tau_1}) - \gamma_3 \bar{M} \tag{0.8}$$

$$CV2: \quad \frac{d\bar{C}}{d\hat{t}} = \theta_3 \bar{A}(\hat{t}-\hat{\tau_2})\bar{S}(\hat{t}-\hat{\tau_2}) - \gamma_4 \bar{C} \tag{0.9}$$

$$ALK1: \quad \frac{d\bar{S}}{d\hat{t}} = \bar{B}(\hat{t}-\hat{\tau_3})^2 - \bar{S} \tag{0.10}$$

0.2.3 Parameter Estimations

Gene expression analysis on cell cultures of HPAECs perturbed by BMP-9 and BMP-4 provide estimations for some of the production rate parameters. BMP-9 induces the expression of MGP and CV2. The respective production rates in the model are k_3 and k_4 with units ng^{-1} ml hr^{-1}. After adding 10 ng^{-1} ml of BMP-9 into the cell culture, MGP expression increased by 1.58 fold in 3 hours, accounting for the 6 hour time delay. Normalizing the rate by the concentration of BMP-9 added to the culture makes $k_3 = 0.053$ ng^{-1} ml hr^{-1}. Similarly, CV2 expression increased by 2.50 fold after 4.33 hours, accounting for the 20 hour time delay, and after normalization yields $k_4 = 0.057$ ng^{-1} ml hr^{-1}.

In another set of experiments the HPAEC culture is treated with 50 ng^{-1} ml of BMP-4 and ALK1 expression increased by 1.82 fold after 9 hours, accounting for the 8 hour time delay. The production rate of ALK1 in the model, k_5 has units ng^{-1} ml hr^{-1} and after normalization by the concentration of BMP-4 added results in $k_5 = 0.004$ ng^{-1} ml hr^{-1}. The experiments did not provide estimates for the growth rate parameters of BMP-9 and BMP-4, k_1 and k_2, respectively, so approximations are made based on the other production rates. The units for k_1 and k_2 are ng ml^{-1} hr^{-1}. The production rate estimate for BMP-4, k_2, is derived from that of ALK1 since both BMP-4 and ALK1

are induced by BMP-4 signaling through its ALK2 receptor. The units are adjusted by multiplying k_4 by the square of the concentration of BMP-4 added, 50 ng^{-1} ml, to obtain $k_2 = 10$ ng ml^{-1} hr^{-1}. The source rate of BMP-9, k_1 also has the same units as k_2 and is estimated to be $k_1 = 5$ ng ml^{-1} hr^{-1}, based on its human vascular circulation rate [34].

The inhibition parameters ρ and ζ are set to 0.9 ng^{-1} ml to approximate an inversely proportional reduction of BMP-4 and BMP-9 with the addition of MGP and CV2, accounting for less than certain inhibition. The final parameter, α, represents the concentration of BMP-4 when its autocatalytic reaction rate is half the maximum rate. Based on a previous study from our lab, we approximate this value to be 20 ng ml^{-1} [37]. The initial conditions for all the simulations are: (BMP-9) A_0 = 10 ng/ml, (BMP-4) B_0 = 50 ng/ml, (MGP) M_0 = 0 ng/ml, (CV2) C_0= 0 ng/ml, (ALK1) S_0 = 50 ng/ml. Table 0.1 summarizes the estimated parameters.

0.2.4 Monte Carlo Parameter Sampling for Oscillations

Constructing mathematical models for biological processes commonly involves many unknown parameters. Paraphrasing Albert Einstein, a model should be as simple as possible, but not simpler. A parsimonious strategy is often utilized since accounting for all mechanisms results in a larger number of variables and uncertain parameters that are difficult to measure experimentally. However, even after reducing a model to one that captures the essential dynamics of the system, many parameters are still unknown. In an effort to better understand the oscillatory conditions for this model we employed uncertainty analysis on the model's equilibrium dynamics by varying the parameter conditions through Monte Carlo (MC) sampling.

MC statistical sampling is employed to evaluate the oscillatory dynamics of the model under random non-dimensional parameter selections. This method provides frequency plots of the parameter values that result in periodic behavior. For each non-

Dimensional Parameters	Value	Units	Function
k_1	5	ng ml^{-1} hr^{-1}	BMP-9 production rate
k_2	10	ng ml^{-1} hr^{-1}	maximum BMP-4 production rate
k_3	0.053	ng^{-1} ml hr-1	MPG production rate
k_4	0.054	ng^{-1} ml hr-1	CV2 production rate
ρ	0.9	ng^{-1} ml	MGP inhibitory coefficient on BMP-4
ζ	0.9	ng^{-1} ml	CV2 inhibitory coefficient on BMP-9
α	20	ng ml^{-1}	BMP-4 concentration at half-maximal autocatalytic reaction rate
μ_1	Unknown	hr^{-1}	BMP-9 degradation rate
μ_2	Unknown	hr^{-1}	BMP-4 degradation rate
μ_3	Unknown	hr^{-1}	MGP degradation rate
μ_4	Unknown	hr^{-1}	CV2 degradation rate
μ_5	1.5	hr^{-1}	ALK1 endocytosis rate
τ_1	6	hr	MGP transcriptional time-delay
τ_2	20	hr	CV2 transcriptional time-delay
τ_3	8	hr	ALK1 transcriptional time-delay
Dimensionless Parameters			
θ_1	9.00		coefficient for BMP-4 autocatalytic saturation
θ_2	1.02		coefficient for MGP production
θ_3	1.10		coefficient for CV2 production
γ_1	Unknown		Relative degradation rate of BMP-9 to ALK1
γ_2	Unknown		Relative degradation rate of BMP-4 to ALK1
γ_3	Unknown		Relative degradation rate of MGP to ALK1
γ_4	Unknown		Relative degradation rate of CV2 to ALK1
$\hat{\tau_1}$	9		MGP transcriptional time-delay
$\hat{\tau_2}$	30		CV2 transcriptional time-delay
$\hat{\tau_3}$	12		ALK1 transcriptional time-delay

Table 0.1: **Model Parameters**: This table contains the approximate values, units, and the biological functions of the dimensional and dimensionless parameters used in this study.

dimensional parameter, random sampling is performed on a log base 10 scale using the uniform distribution on the interval [-3 to 3]. The logarithmic scale is used to prevent undersampling of values on the outer ranges of the intervals, since each non-dimensional parameter is a ratio of dimensional parameters. The log base 10 range of [-3, 3] corresponds to a parameter ratio range of [0.001, 1,000], covering seven orders of magnitude. For example, if $\mu_1 = 0.01$ ($log_{10}(0.01) = -2$), ALK1 is degraded 100 times faster than BMP-9. Alternatively, a value of 100 ($log_{10}(100) = 2$) corresponds to an ALK1 degradation that is 100 times slower than that of BMP-9. For each set of randomly selected parameters the model output is analyzed for the presence of periodic dynamics.

It is computational very expensive to perform linear stability and eigenvalue analysis for time-delay differential equations numerous times for MC sampling, so instead we use a numerical approach to detect the oscillations in the model output. For each simulation we independently sample the 4 non-dimensional degradation parameters and numerically solve the time-delay differentially equations for 2,000 time-steps using the NDSolve function in $Mathematica$. We extract the final 200 time-steps, $\mathbf{t}_f$, for each variable so that the initial transient behavior of the model is ignored and the steady state stability conditions can be observed. This data is normalized against its maximum value during that time-interval for each variable.

To identify oscillatory dynamics, we calculate the variance of $\mathbf{t}_f$. In the case of a stable system $var(\mathbf{t}_f) \approx 0$. For periodic behavior and non-oscillatory unstable behavior we expect $var(\mathbf{t}_f) > 0$ since the output is either fluctuating or exponentially growing. We numerically set a threshold variance, $var_{thresh} = 0.01$, and if $var(\mathbf{t}_f) < var_{thresh}$ we consider the output as a stable node. If $var(\mathbf{t}_f) > var_{thresh}$, we calculate the discrete derivative $\delta_{\mathbf{t}_f}(i) = \frac{\mathbf{t}_f(i+\Delta) - \mathbf{t}_f(i)}{\Delta}$ for each variable output, with $\Delta = 1$ for i = 1 to 199.

In the case of an unstable non-oscillatory node, $\delta_{\mathbf{t}_f}$ should be positive for all i, while for an oscillating output $\delta_{\mathbf{t}_f}$ should have a mixture of positive and negative val-

ues. We define the fraction of negative values for $\delta_{\mathbf{t}_f}$ compared to positive values as δ_{frac}. If $var(\mathbf{t}_f) > var_{thresh}$ and $\delta_{frac} \leq 0.05$, the output is considered unstable and non-oscillatory. If $var(\mathbf{t}_f) > var_{thresh}$ and $\delta_{frac} > 0.05$, the output is considered oscillatory. This numerical method resulted in zero parameter conditions yielding unstable exponentially growing outputs, as expected for a biological model. While we can characterize the dynamics of the model output relatively quickly without performing stability analysis on each equilibrium point, this method has difficulty differentiating between slowly decaying stable spirals, and limit cycles. However, for our practical purpose of modeling experiments with finite time, capturing slowly decaying spirals is still of value.

0.2.5 Hopf Bifurcation Analysis of Delay-Differential Equations

The MC global parameter analysis identifies approximate parameter regimes for which oscillations occur in this model. The parameters with narrower distributions require more specific values for the creation of oscillations. This technique is useful for obtaining a general understanding of parameters with sensitive ranges for oscillation, but it is of interest to explore more specific conditions leading to periodic behavior. This is done using linear stability analysis on the equilibrium points of the time-delay differential equations.

The equilibrium points for the model are points in variable state space for which all the differential equations are equal to zero. In vector notation, $\mathbf{x}(t) = \mathbf{x}^*$ is the vector of equilibrium points such that $f(\mathbf{x}^*) = 0$, where $f(\mathbf{x})$ is the system of delay differential equations. Stability analysis with ODEs involves a finite-dimensional coordinate space, while DDEs are contained within an infinite-dimensional phase space. Displacements from the equilibrium point $\delta\mathbf{x}(t)$ occur up to the longest time-delay, τ_{max}. In order for the equilibrium point to be stable, it must be stable in the presence of perturbations occurring during its recent history, going back to $t - \tau_{max}$ [38].

For notational purposes, instantaneous variables will be indicated as $\mathbf{x} = \mathbf{x}(t)$ and delayed variables as $\mathbf{x}_\tau = \mathbf{x}(t-\tau)$. If the equilibrium point is perturbed by $\delta\mathbf{x}(t)$ along the interval $[t-\tau_{max}, \infty)$, then

$$\mathbf{x} = \mathbf{x}^* + \delta\mathbf{x} \tag{0.11}$$

and its derivative is

$$\dot{\mathbf{x}} = \dot{\delta\mathbf{x}} = f(\mathbf{x}^* + \delta\mathbf{x}, \mathbf{x}^* + \delta\mathbf{x}_{\tau_1}, \mathbf{x}^* + \delta\mathbf{x}_{\tau_2}, \mathbf{x}^* + \delta\mathbf{x}_{\tau_3}) \tag{0.12}$$

accounting for the three time delays. Applying the Taylor series method to linearize Equation (0.12) about the equilibrium point yields

$$\dot{\delta\mathbf{x}} \approx f(\mathbf{x}^*) + J_0\delta\mathbf{x} + J_{\tau_1}\delta\mathbf{x}_{\tau_1} + J_{\tau_2}\delta\mathbf{x}_{\tau_2} + J_{\tau_3}\delta\mathbf{x}_{\tau_3}. \tag{0.13}$$

By definition, the differential equations evaluated at the equilibrium point equal zero, $f(\mathbf{x}^*) = 0$, simplifying Equation (0.13) to

$$\dot{\delta\mathbf{x}} \approx J_0\delta\mathbf{x} + J_{\tau_1}\delta\mathbf{x}_{\tau_1} + J_{\tau_2}\delta\mathbf{x}_{\tau_2} + J_{\tau_3}\delta\mathbf{x}_{\tau_3}. \tag{0.14}$$

In this equation, J_0 is the Jacobian of $f(\mathbf{x}, \mathbf{x}_{\tau_1}, \mathbf{x}_{\tau_2}, \mathbf{x}_{\tau_3})$ with respect to $\mathbf{x}$ and J_{τ_n} is the Jacobian with respect to $\mathbf{x}_{\tau_n}$.

Assuming the differential equation has a solution of the form

$$\delta\mathbf{x} = \mathbf{A}e^{\lambda t}, \quad \delta\mathbf{x}_{\tau_n} = \mathbf{A}e^{\lambda(t-\tau_n)}, \tag{0.15}$$

and applying this to Equation (0.14), we get

$$\lambda \mathbf{A} e^{\lambda t} \approx J_0 \mathbf{A} e^{\lambda t} + J_{\tau_1} \mathbf{A} e^{\lambda (t-\tau_1)} + J_{\tau_2} \mathbf{A} e^{\lambda (t-\tau_2)} + J_{\tau_3} \mathbf{A} e^{\lambda (t-\tau_3)}. \tag{0.16}$$

Simplifying this expression yields

$$\begin{aligned} \lambda \mathbf{A} &= (J_0 + e^{-\lambda \tau_1} J_{\tau_1} + e^{-\lambda \tau_2} J_{\tau_2} + e^{-\lambda \tau_3} J_{\tau_3}) \mathbf{A} && (0.17) \\ 0 &= (J_0 + e^{-\lambda \tau_1} J_{\tau_1} + e^{-\lambda \tau_2} J_{\tau_2} + e^{-\lambda \tau_3} J_{\tau_3} - \lambda \mathbf{I}) \mathbf{A}. && (0.18) \end{aligned}$$

The presence of a nonempty kernel for the matrix in (0.18) indicates its determinant equals 0, thus providing the characteristic equation

$$|\mathbf{J}_0 + e^{-\lambda \tau_1} \mathbf{J}_{\tau_1} + e^{-\lambda \tau_2} \mathbf{J}_{\tau_2} + e^{-\lambda \tau_3} \mathbf{J}_{\tau_3} - \lambda \mathbf{I}| = 0 \tag{0.19}$$

where $\mathbf{I}$ is the identity matrix. The characteristic equation (0.19) is transcendental with an infinite number of solutions due to the presence of exponential terms. For the system to be stable all real parts of the eigenvalues, λ, must be negative. A positive real component indicates an unstable equilibrium point. A Hopf bifurcation occurs when the eigenvalue crosses the vertical axis, transitioning from a negative to positive real part of the complex conjugate eigenvalues. Linearization is performed on all equilibrium points to determine their stability. Unlike MC sampling, Hopf bifurcation analysis can differentiate between equilibrium point stability types, including stable and unstable spiral nodes. The $Mathematica$ software program is used for computing the equilibrium points, solving the Jacobian Matrix, and finding the eigenvalues from the characteristic equation.

0.2.6 Cell Culture Experiments

We closely collaborated with the Bostrom Lab at UCLA who conducted cell culture experiments on this BMP system. Human pulmonary artery endothelial cells (HPAECs) were prepared and cultured on 12-well plates at day 0. There were approximately 20,000 cells/well. At day zero, the wells were divided into 4 treatment groups: addition of BMP-9 (10 ng/ml), BMP-4 (50 ng/ml), anti-BMP-9 + Noggin (100 ng/ml), and a control group with nothing added. After the initial treatment, samples were collected approximately every 8 hours for 6 days and real-time PCR analysis was performed to measure gene expression levels of ALK1, MGP, CV2, and CD34. The data was normalized to reflect relative expression fold changes based on the initial mRNA quantity detected per molecule.

0.3 Results

0.3.1 Monte Carlo Simulation

The MC parameter sampling allowed us to globally identify the differential equation parameter regimes yielding oscillatory outputs. We ran the simulation 2,000 times, independently random sampling the parameters γ_1, γ_2, γ_3, and γ_4 with replacement on each run. Consequently there is a 4-element vector, **p**, containing the parameters being resampled on each run. The dimensionless parameters simplify the interpretation of the results to relativistic comparisons of dimensional parameters. Of the 2,000 simulations, 53 resulted in oscillatory behavior (1.8%). Figure 0.7 shows the parameter distributions for oscillations in this model.

Of the four degradation parameters, those for BMP-9, BMP-4, and MGP showed a bias towards lower ratio values in the presence of oscillations. Due to the lack of normality in the skewed distributions, the median is a better measure of center than the mean. For γ_1, the relative degradation rate of BMP-9 to ALK1, the range of log values yielding oscillation is $[-2.98, 2.47]$ with a median of -1.90 (-2.35, -1.53, 95% C.I.) (Table 0.3). The median log γ_1 value of -1.90 corresponds to the degradation rate of ALK1 that is 79.4 times faster than the degradation rate of BMP-9. The median C.I. does not intersect the log-ratio of equality, 0, indicating that the center of the γ_1 distribution is biased towards lower relative degradation rates of BMP-9. High BMP-9 degradation rates do not favor oscillatory activity because BMP-9 must be present to induce expression of MGP and CV2 for feedback regulation.

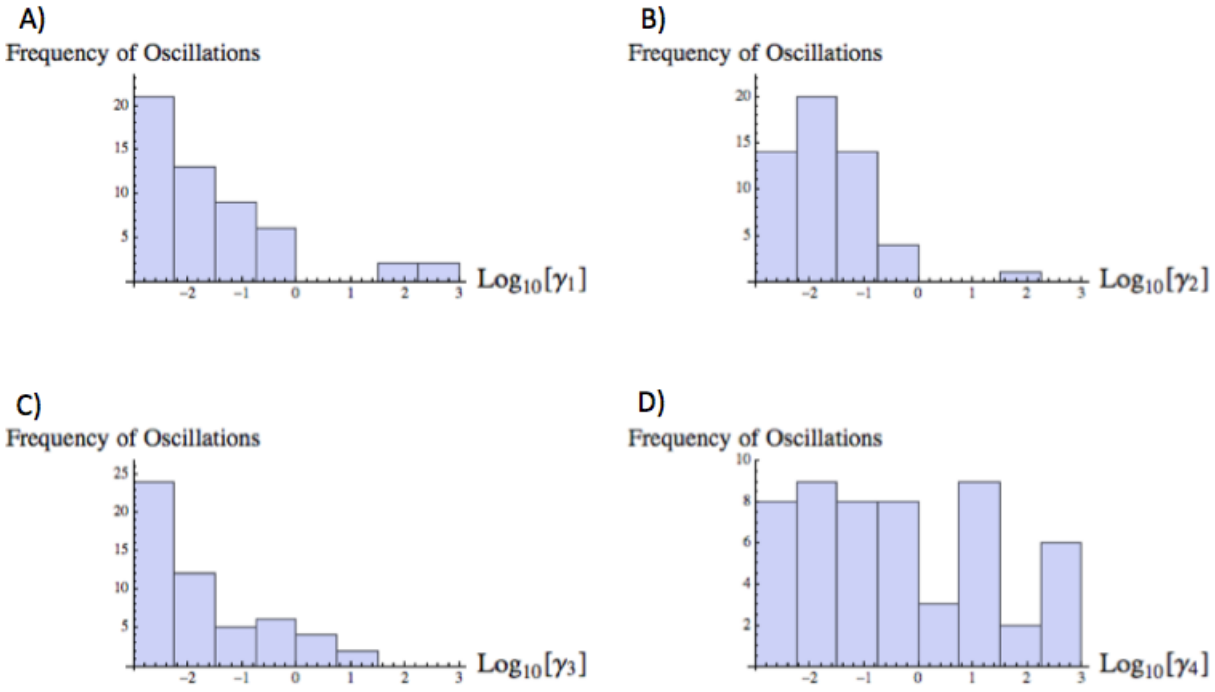


Figure 0.7: **MC sampling parameter distributions**: the log parameter distributions that result in an oscillatory model output. A) γ_1, B) γ_2, C) γ_3, D) γ_4.

The degradation rate of BMP-4, γ_2, is also skewed to log values less than 0. Its distribution ranges from $[-2.65, 1.54]$ with a median of -2.02 $(-2.13, -1.52)$. However, only 1 of the 53 parameters has a log value greater than 0. Thus, the presence of oscillatory dynamics highly favors the degradation of BMP-4 to be less than the degradation rate of ALK1. If BMP-4 is degraded too quickly, it cannot adequately induce ALK1 expression for BMP-9/ALK1 signaling. We expect the elimination rate for BMP-4 and BMP-9 to be roughly less than or equal to the endocytosis rate of ALK1 since their primary mechanism of degradation is through BMP-bound receptor endocytosis [30].

The relative MGP degradation rate, γ_3, distribution has a range of $[-2.99, 1.07]$ with median of -2.13 $(-2.44, -1.62)$. The median C.I. does not contain 0, reflecting the oscillatory bias for a lower MGP elimination rate compared to ALK1. If MGP is degraded greater than 11 times faster than ALK1, the negative feedback signal on

Parameter (p)	Median ($log_{10}(p)$)	Median 95% C.I.	Range
γ_1	-1.90	(-2.36, -1.53)	[-2.98, 2.47]
γ_2	-2.02	(-2.14, -1.52)	[-2.66, 1.54]
γ_3	-2.13	(-2.44, -1.62)	[-2.99, 1.07]
γ_4	-0.58	(-1.10, 0.21)	[-2.68, 2.62]

Table 0.2: **MC sampling parameter distribution statistics with fixed delays**: the median values, median 95% C.I., and the range for each parameter distribution.

BMP-4 is not strong enough to induce periodic behavior. Its presence as a negative feedback regulator of BMP-4 is thus critical for oscillations. The true value of γ_3 is expected to be less than 1 since MGP is degraded slowly as a result of its positioning in the extracellular matrix [28]. The distribution of γ_4, for the degradation rate of CV2, has a log range of $[-2.68, 2.62]$ and a median of -0.58 $(-1.10, 0.21)$. Compared to the other parameters, γ_4, induces oscillations for a more evenly distributed set of values. The log median C.I. contains 0, reflecting the lack of a strong oscillatory bias to low or high relative CV2 degradation rates. Since CV2 is a soluble protein, it is expected to be eliminated faster than BMP-4, BMP-9, and MGP.

We also investigated the impact of uncertainty in the time-delays on the MC distribution results. The experimental gene transcription time-delays are normally distributed with a mean equal to the peak delay, τ_n, and a standard deviation equal to 10% of τ_n [32]. The probability density function for each τ is plotted in Figure 0.8.

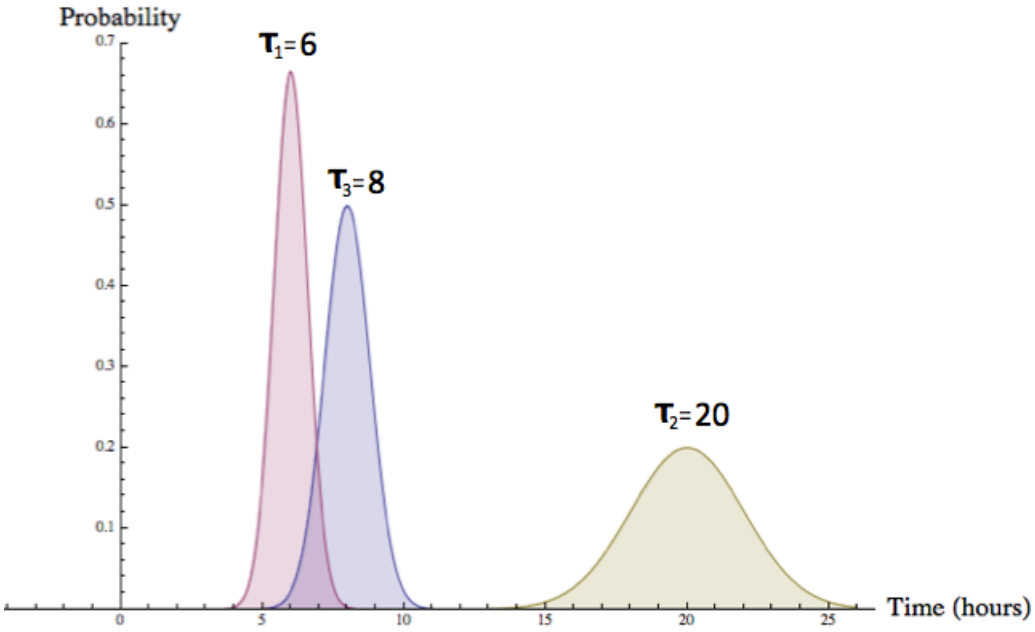


Figure 0.8: **Time-delay probability density functions**: the normal distributions are defined with a mean equal to the peak time delay, τ_n and a standard deviation equal to 10% τ_n. These distributions are used for MC sampling.

We performed MC sampling on the γ parameters like before, except now we sampled the time-delays from their respective normal distributions instead of designating them with a fixed value. The resulting MC distributions (Figure 0.9) are very similar to Figure 0.7. BMP-9, BMP-4, and MGP are biased towards lower relative degradation rates, while CV2 is not. This indicates that the uncertainty in the time-delays does not dramatically change the MC simulation results making it reasonable to approximate the time-delays with discrete constants instead of random variables.

Parameter (p)	Median ($log_{10}(p)$)	Median 95% C.I.	Range
γ_1	-1.89	(-2.38, -1.04)	[-2.93, 0.22]
γ_2	-1.76	(-2.26, -1.20)	[-2.81, 2.50]
γ_3	-2.11	(-2.51, -1.56)	[-2.97, 1.16]
γ_4	-0.32	(-1.03, 1.04)	[-2.51, 2.81]

Table 0.3: **MC sampling parameter distribution statistics with a normally distributed delays**: the median values, median 95% C.I., and the range for each parameter distribution. The time-delays are randomly sampled from normal distributions centered around τ_n.

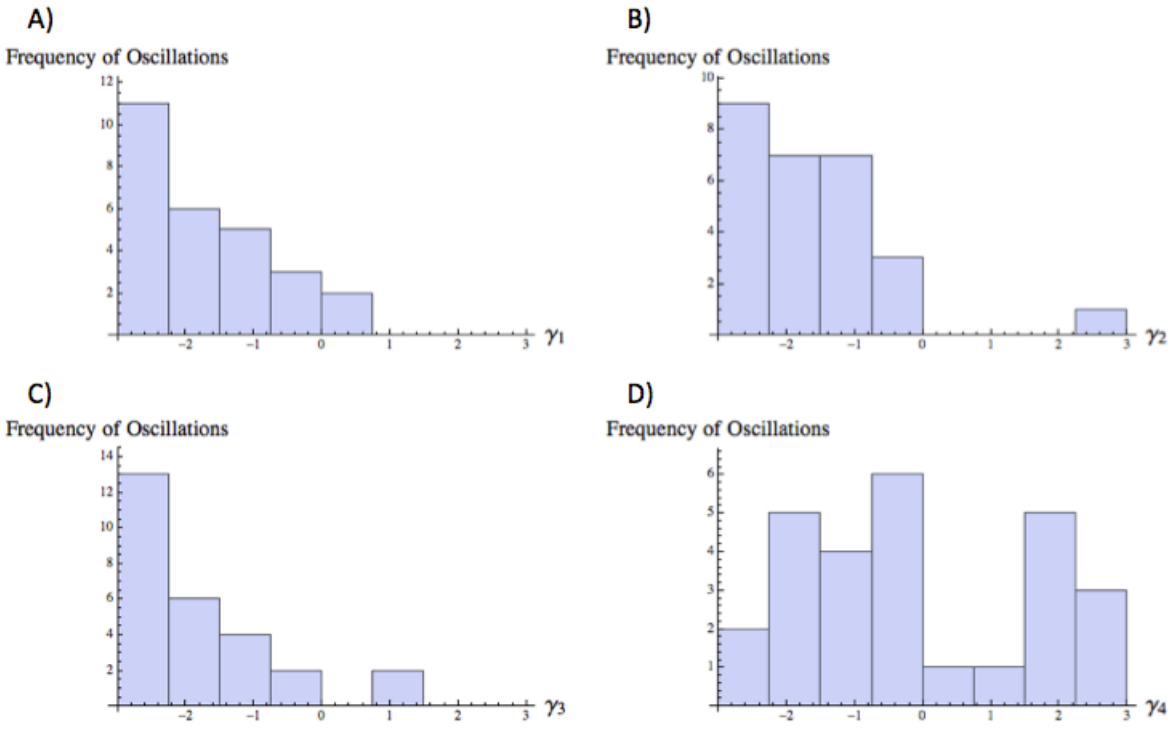


Figure 0.9: **Time-delay probability density functions**: the normal distributions are defined with a mean equal to the peak time delay, τ_n and a standard deviation equal to 10% τ_n. These distributions are used for MC sampling.

Central take-home points from MC parameter sampling:

- Oscillations prefer:

  1. BMP-9 degradation $<$ ALK1 degradation

2. BMP-4 degradation $<$ ALK1 degradation

3. MGP degradation $<$ ALK1 degradation

4. CV2 degradation can greatly vary relative to ALK1 degradation

- Uncertainty in time-delays, τ_n, does not significantly alter MC results.

0.3.2 1-Parameter Hopf Bifurcation Analysis

MC sampling of the parameter space provides an approximate global understanding of the parameter distributions in the presence of oscillatory activity. It is of interest to more thoroughly investigate how the model transitions into different stability regimes as parameters are adjusted. To do so, we perform linear stability analysis on the equilibrium points of the model while adjusting 1 or 2 degradation parameters and keeping the rest constant.

0.3.2.1 BMP-4 Degradation

First we will explore the implications of changing the degradation rate of BMP-4, γ_2, while keeping the other parameters fixed. Since BMP-9 is primarily degraded through endocytosis when bound to ALK-1, we approximate μ_1 as $\frac{1}{10} \cdot \mu_5$, and thus $\gamma_2 = 0.1$ to account for the fraction bound being degraded. We also assume there much is more ALK1 in the system compared to BMP-9 to avoid saturation. This is a reasonable assumption due to the high initial ALK1 mRNA quantity in the control HPAEC culture. MGP is a constituent member of the extracellular matrix causing it to be degraded slowly. We set its rate to be slower than μ_5 with a value $\gamma_3 = 0.5$. CV2 is a soluble protein whose degradation rate is set to be on the same order as ALK1, $\gamma_4 = 1$.

We perturb γ_2 from a log value of -3 to 3 incrementing by steps of 0.05 to cover the conditions when BMP-4 degradation is 3 orders of magnitude less than to 3 orders of magnitude greater than ALK1 degradation. As γ_2 is increased the system transitions

from 3 to 1 equilibrium points (Figure 0.10). This diagram plots the parameter γ_2 against the equilibrium points of BMP-9, BMP-4, MGP, and CV2. The red points represent stable equilibrium with $Re(\lambda) < 0$, where λ is the eigenvalue of the equilibrium point. Blue points are unstable equilibrium points with $Re(\lambda) > 0$. The consistently red equilibrium trace is stable for all values of γ_2 explored. There are two curved equilibrium traces with one portion being unstable throughout and the other bifurcating from stable to unstable before annihilating with the other unstable point.

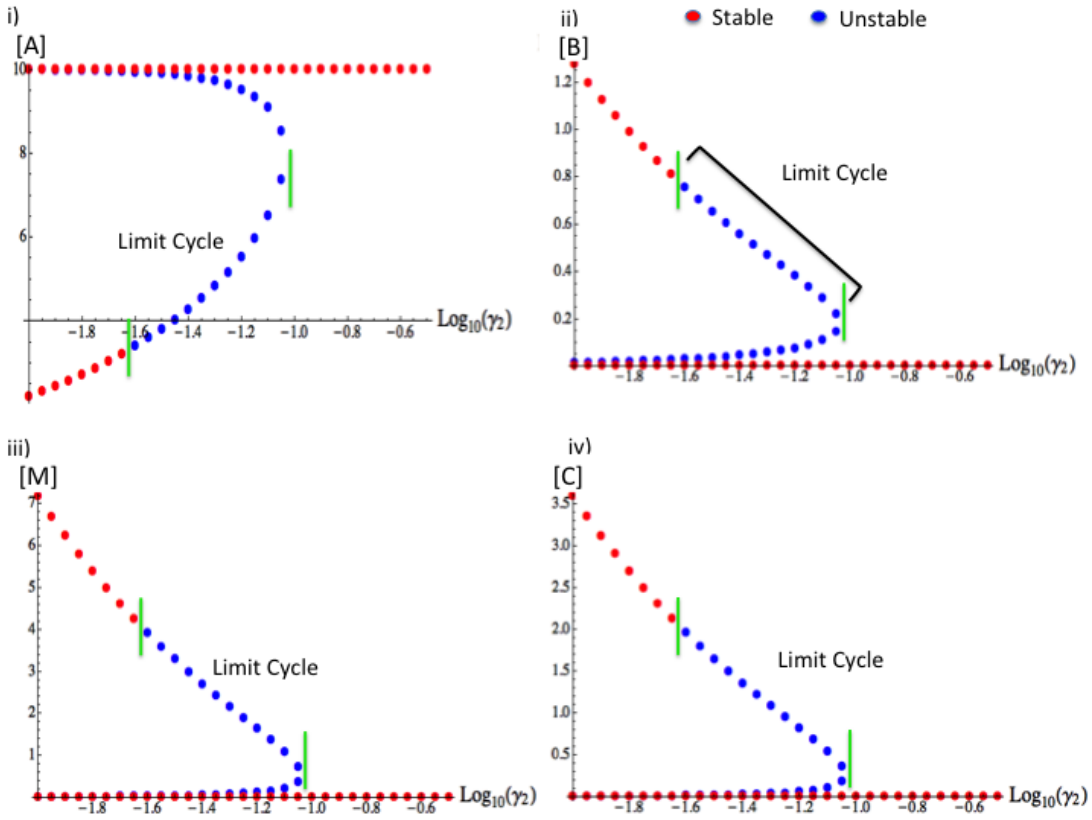


Figure 0.10: **BMP-4 degradation rate (γ_2) equilibrium point stability diagram** : The x-axis contains the parameter value and the y-axis represents the equilibrium points of the non-dimensional variables A= BMP-9, B= BMP-4, M=MGP, C = CV2. Red and blue dots symbolize stable and unstable equilibrium points, respectively. The green lines mark the boundary of the parameter regime exhibiting limit cycle dynamics.

The consistently stable equilibrium point is a stable node with $Re(\lambda) < 0$ and $Im(\lambda) = 0$. The consistently unstable equilibrium point is an unstable node with

$Re(\lambda) > 0$ and $Im(\lambda) = 0$. As γ_2 increases from $log_{10}(\gamma_2) = -1.65$ to -1.60, the third equilibrium point has a complex conjugate eigenvalue that transitions from $Re(\lambda) < 0$ to $Re(\lambda) > 0$. Unlike regular ODEs, DDEs have a transcendental characteristic equation with an infinite number of roots [39]. The numerical solution for the characteristic equation at $log_{10}(\gamma_2) = -1.60$ indicates that the largest $Re(\lambda)$ is positive, making the equilibrium point an unstable spiral (Figure 0.11 part A). This is a supercritical Hopf bifurcation, which occurs when a stable spiral changes into an unstable spiral surrounded by a limit cycle [40]. This bifurcation is visible in the time series plot in Figure 0.12. Before the Hopf bifurcation when $log_{10}(\gamma_2) = -1.65$ the 5 variables exhibit damped oscillations. After the bifurcation when $log_{10}(\gamma_2) = -1.60$ the variables are oscillating in a limit cycle.

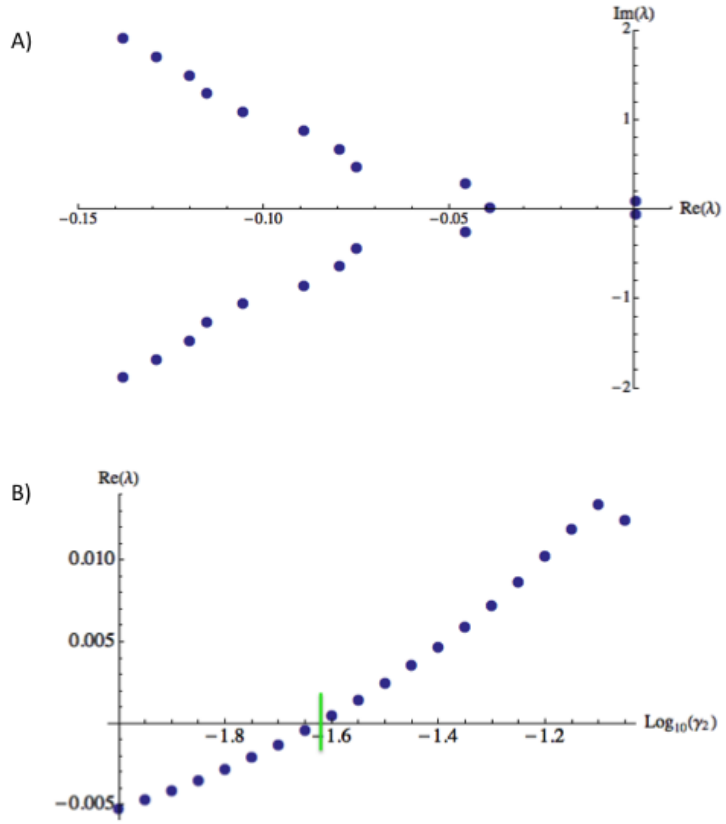


Figure 0.11: **BMP-4 degradation rate (γ_2) eigenvalue analysis for the equilibrium point exhibiting a Hopf bifurcation**: A) The eigenvalues of the transcendental characteristic equation after the Hopf bifurcation ($log_{10}(\gamma_2) = -1.6$). The rightmost complex conjugate eigenvalue has a positive real part indicating an unstable spiral equilibrium point. B) The real component of the eigenvalue for the equilibrium point undergoing the Hopf bifurcation as γ_2 is changed. This is the same eigenvalue for variables A, B, M, C, and S. There is a supercritical Hopf bifurcation (marked by green lines) and an equilibrium point annihilation.

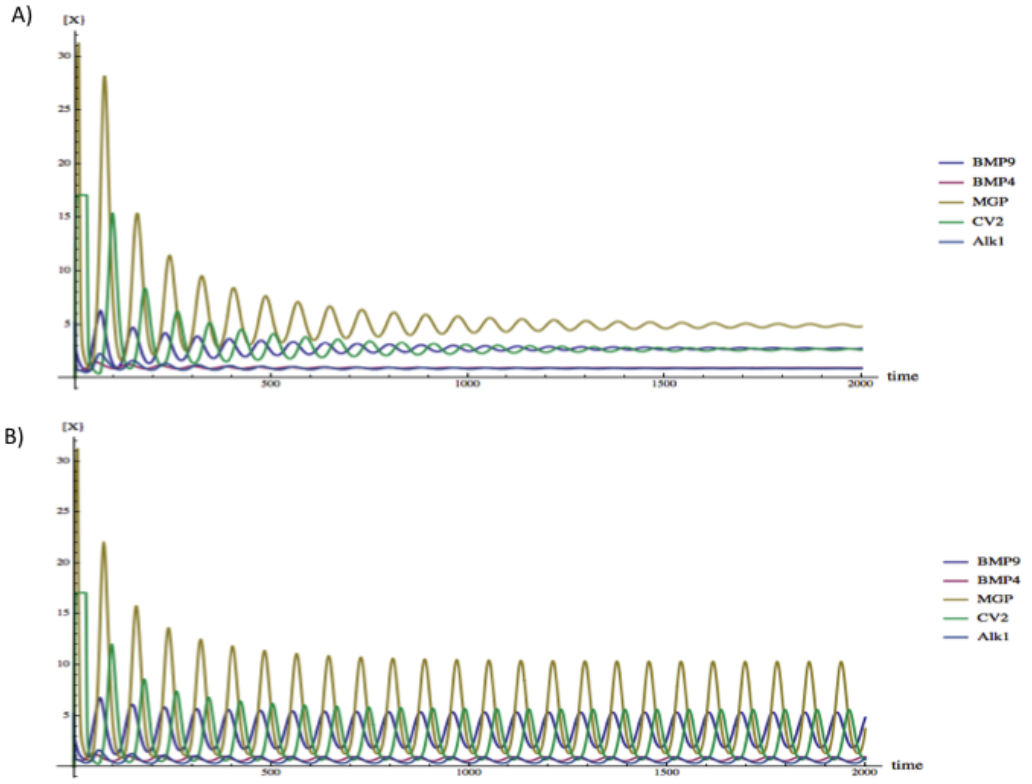


Figure 0.12: **Limit cycle in time series**: A) The spiraling stable dynamics of the model before the Hopf bifurcation ($log_{10}(\gamma_2) = -1.65$). B) The limit cycle dynamics of the model after the Hopf bifurcation ($log_{10}(\gamma_2) = -1.6$). A = BMP-9, B = BMP-4, M=MGP, C=CV2, S=ALK1.

As γ_2 continues to increase, the unstable spiral node that gives rise to a limit cycle encounters another bifurcation. When $log_{10}(\gamma_2) = -1$ the two unstable nodes collide and annihilate each other, leaving 1 stable equilibrium point. This bifurcation eliminates oscillations and causes the system to reach a stable steady-state equilibrium point. As a result, there is a bounded region of oscillatory dynamics between the two bifurcations. This is visible in Figure 0.11 part B when the $Re(\lambda) > 0$. The first Hopf bifurcation occurs when the eigenvalue crosses the x-axis at $\gamma_2 = log_{10}(-1.6)$ and the second bifurcation occurs when the equilibrium point disappears at $log_{10}(\gamma_2) = -1$. The BMP-4/9 network exhibits periodic behavior when the degradation of BMP-4 is 10 to 40 times slower than the degradation rate of ALK1. If the degradation rate is too

fast, there is not enough BMP-4 present to induce oscillations.

0.3.2.2 BMP-9 Degradation

The model exhibits similar dynamics when the relative degradation rate of BMP-9, γ_1, is perturbed. A degradation rate is greater than $log_{10}(\gamma_1) = -1.85$ results in three equilibrium points with the same dynamical properties described previously for BMP-4 degradation. However, the sequence of the two bifurcations occurs in the opposite order compared to γ_2 (Figure 0.13). When γ_2 is decreased below $log_{10}(\gamma_1) = -0.20$ the stable spiral equilibrium point undergoes a supercritical Hopf bifurcation (Figure 0.14), corresponding to a degradation rate that is 1.6 times slower than ALK1 degradation. The limit cycle exists until $log_{10}(\gamma_1) < -0.85$, which is when the unstable spiral node and unstable node collide and destroy each other. Beyond this point the steady-state expression of BMP-9 approaches its source rate, while the other variables decay to 0. The γ_1 parameter range containing limit cycle dynamics is $[log_{10}(-0.85), log_{10}(-0.2)]$, corresponding to a rate that is 7.1 to 1.6 times slower than ALK1 endocytosis. This range consists of faster degradation rates compared to γ_2, suggesting that a longer presence of BMP-4 compared to BMP-9 is important for allowing oscillations.

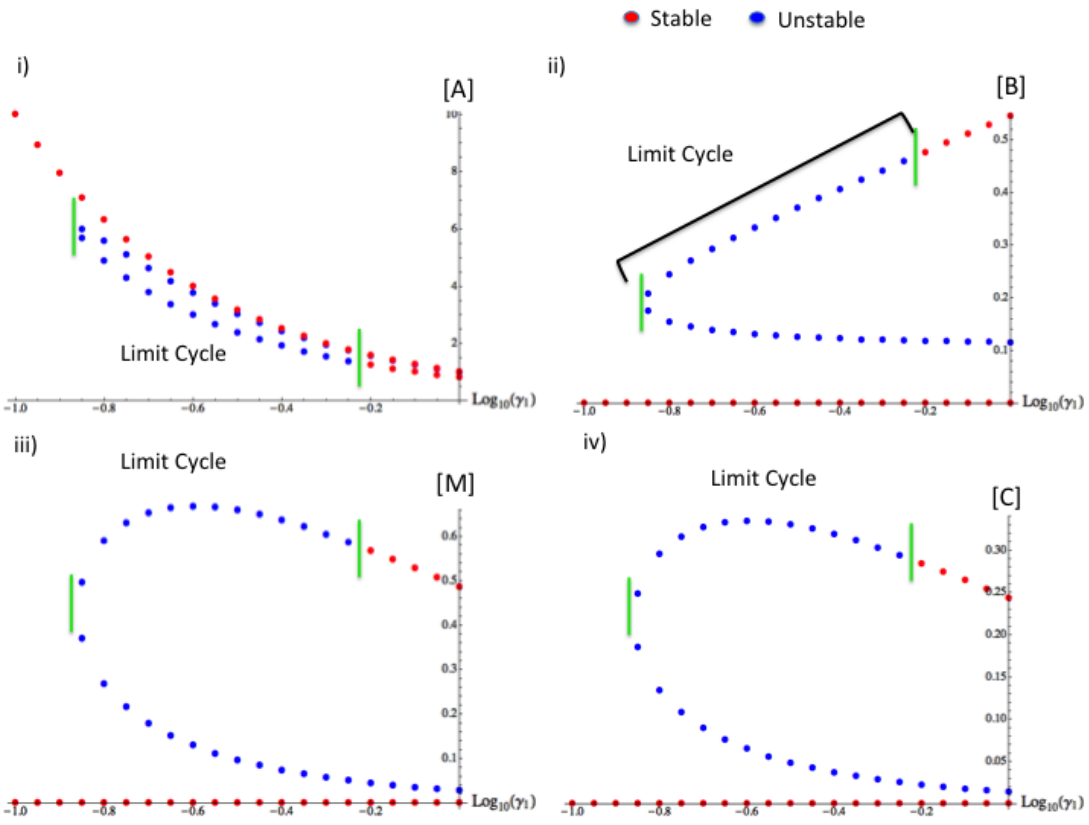


Figure 0.13: **BMP-9 degradation rate (γ_1) equilibrium point stability diagram** : The x-axis contains the parameter value and the y-axis represents the equilibrium points of the non-dimensional variables A= BMP-9, B= BMP-4, M=MGP, C = CV2. Red and blue dots symbolize stable and unstable equilibrium points, respectively. The green lines mark the boundary of the parameter regime exhibiting limit cycle dynamics.

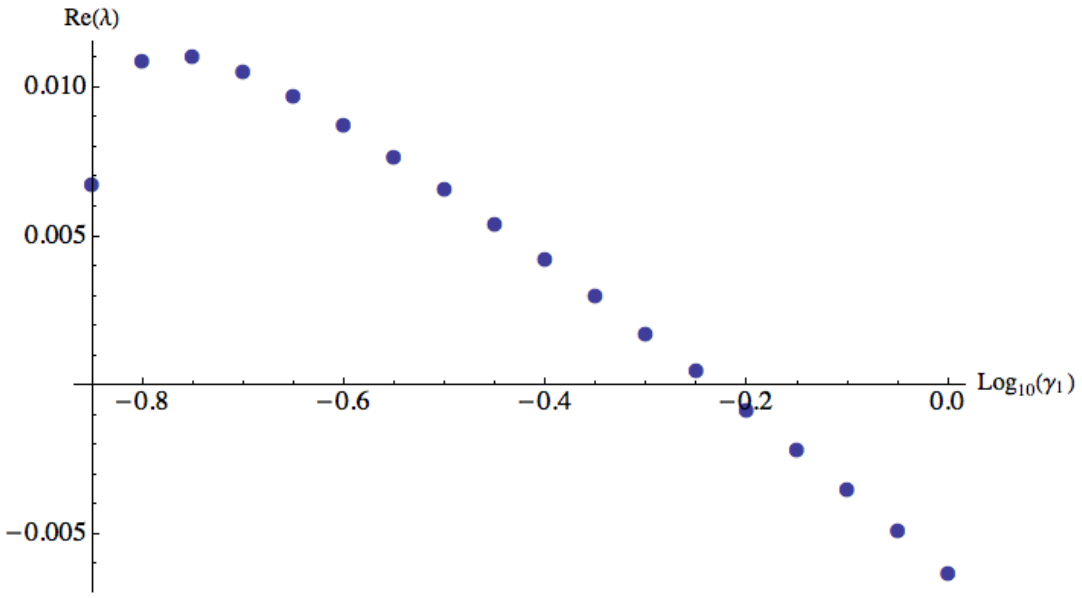


Figure 0.14: **BMP-9 degradation rate (γ_1) eigenvalue analysis for the equilibrium point exhibiting a Hopf Bifurcation**: The real component of the eigenvalue for the equilibrium point undergoing the Hopf bifurcation as γ_1 is changed. This is the same eigenvalue for variables A, B, M, C, and S. There is a supercritical Hopf bifurcation and an equilibrium point annihilation.

0.3.2.3 MGP Degradation

Adjustments in the degradation rate of MPG, the inhibitor of BMP-4, resulted in the same bifurcations seen previously, except in the opposite order compared to γ_2 (Figure 0.15). When $log_{10}(\gamma_3) > 0.55$ there are three equilibrium points, a stable node, unstable node, and stable spiral. A supercritical Hopf bifurcation occurs when $log_{10}(\gamma_3) < 0.55$ (Figure 0.16). This transition creates a limit cycle that persists until $log_{10}(\gamma_3) < -0.15$, which is when the two unstable equilibrium points are destroyed in another bifurcation. Periodic behavior can exist when the degradation rate of MGP is 1.4 times slower to 3.5 times faster than the degradation rate of ALK1. The model favors relatively faster elimination of MGP compared to BMP-4 and BMP-9 for oscillations to exist. If MGP stays around too long, its inhibition of BMP-4 activity shuts off oscillations.

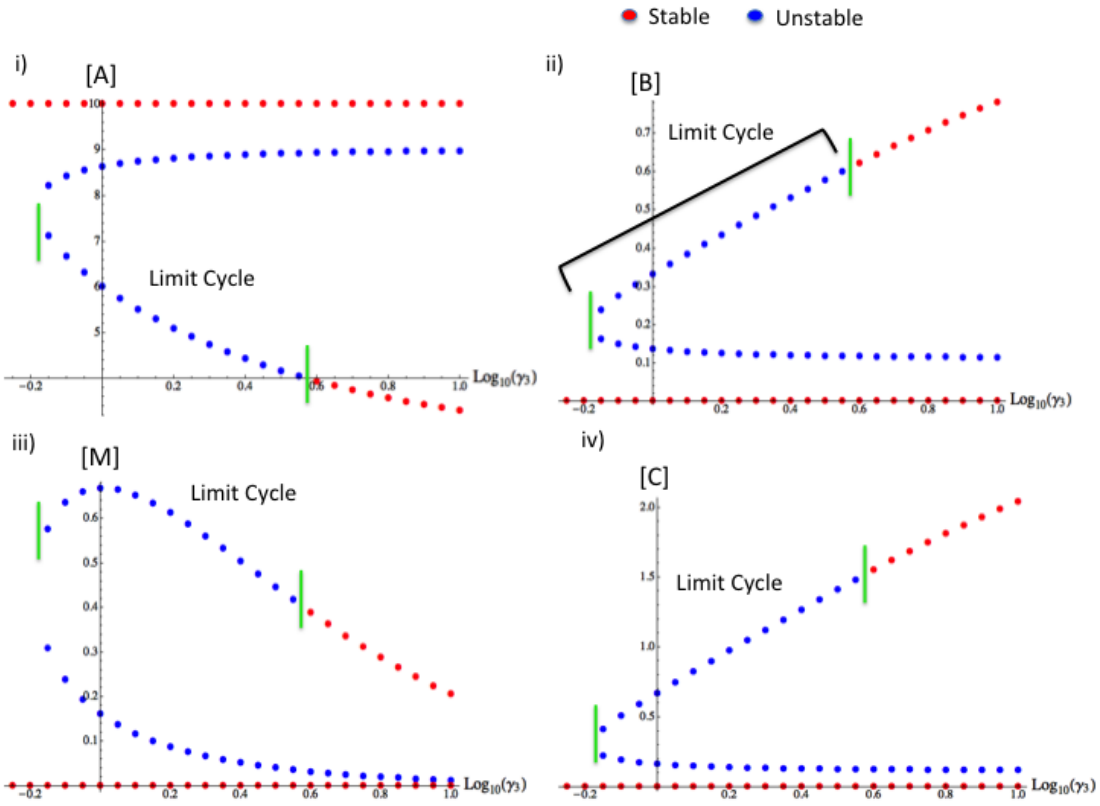


Figure 0.15: **MGP degradation rate (γ_3) equilibrium point stability diagram** : The x-axis contains the parameter value and the y-axis represents the equilibrium points of the non-dimensional variables A= BMP-9, B= BMP-4, M=MGP, C = CV2. Red and blue dots symbolize stable and unstable equilibrium points, respectively. The green lines mark the boundary of the parameter regime exhibiting limit cycle dynamics.

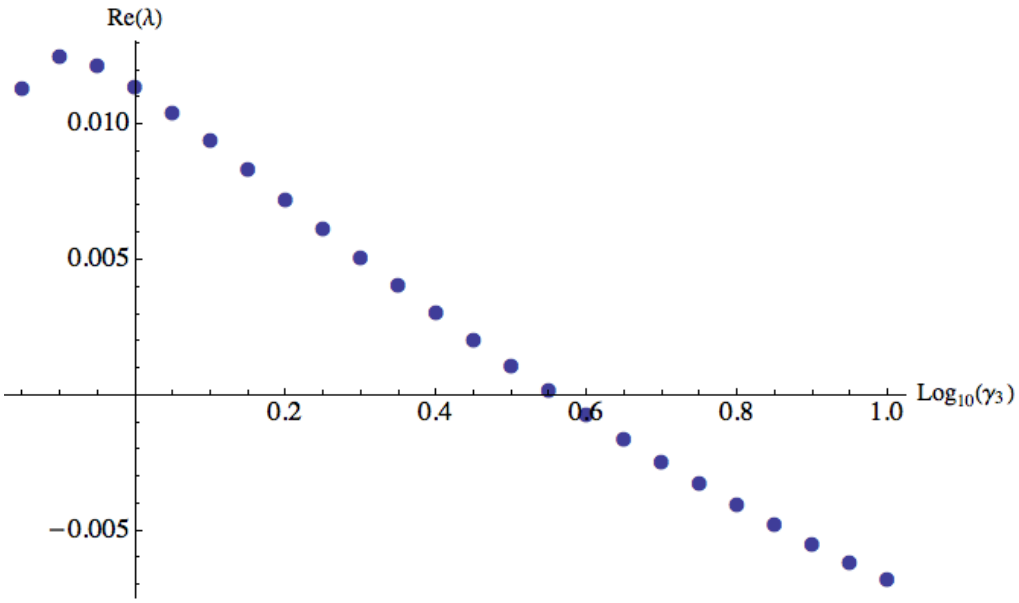


Figure 0.16: **MGP degradation rate (γ_3) eigenvalue analysis for the equilibrium point exhibiting a Hopf Bifurcation**: The real component of the eigenvalue for the equilibrium point undergoing the Hopf bifurcation as γ_3 is changed. This is the same eigenvalue for variables A, B, M, C, and S. There is a supercritical Hopf bifurcation and an equilibrium point annihilation.

0.3.2.4 CV2 Degradation

Changes to the degradation rate of CV2, the inhibitor of BMP-9, also resulted in Hopf bifurcations. Unlike the other decay rates, bifurcations induced by γ_4 do not create or destroy equilibrium points. When $log_{10}(\gamma_4) < -1.2$ the model has a stable node, an unstable node, and a stable spiral (Figure 0.17). The unstable spiral undergoes a supercritical Hopf bifurcation when $log_{10}(\gamma_4) = -1.2$ and enters a limit cycle regime until $log_{10}(\gamma_4) > 0.20$, when it undergoes a reverse Hopf bifurcation to become a stable spiral once again (Figure 0.18). Periodic behavior exists when CV2 degradation is 15.8 times slower to 1.6 times faster than the endocytosis rate of ALK1. Along this equilibrium point, slower CV2 degradation corresponds to higher BMP-4 and CV2 concentrations and lower BMP-9 and MGP concentrations. Similarly, as CV2 degradation is increased, BMP-4 and CV2 concentrations are reduced while BMP-9 and MGP concentrations rise. A greater presence of CV2 indirectly causes higher BMP-4 con-

centrations because of its inhibitory action on BMP-9, leading to less expression of BMP-4 antagonist, MGP.

Based on the 1-parameter linear stability analysis, limit cycles exist when BMP-4 is degraded 40-10 times slower than ALK1, BMP-9 is degraded 7.6-1.6 times slower than ALK1, MGP is degraded 1.4 times slower to 3.5 times faster than ALK1, and CV2 is degraded 15.8 times slower to 1.6 times faster than ALK1. Therefore, the presence of BMP-4 is the most significant for oscillations, followed by CV2, BMP-9, and MGP.

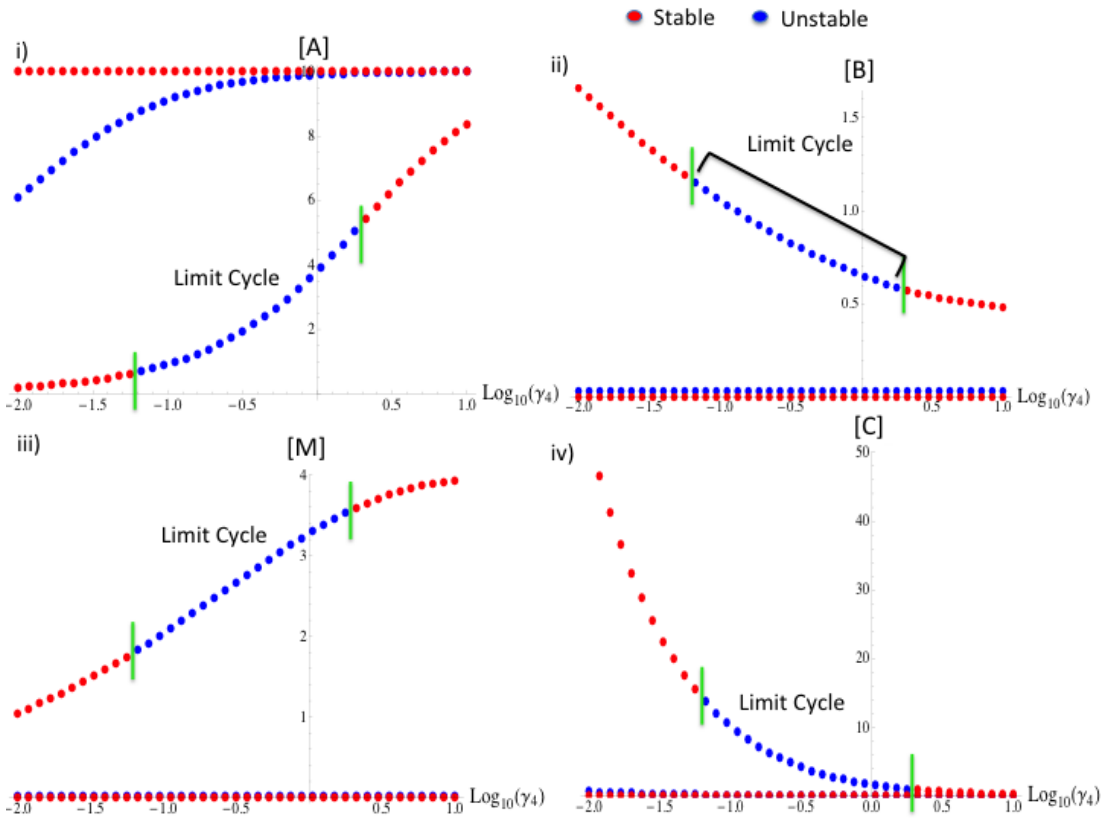


Figure 0.17: **CV2 degradation rate (γ_4) equilibrium point stability diagram** : The x-axis contains the parameter value and the y-axis represents the equilibrium points of the non-dimensional variables A= BMP-9, B= BMP-4, M=MGP, C = CV2. Red and blue dots symbolize stable and unstable equilibrium points, respectively. The green lines mark the boundary of the parameter regime exhibiting limit cycle dynamics.

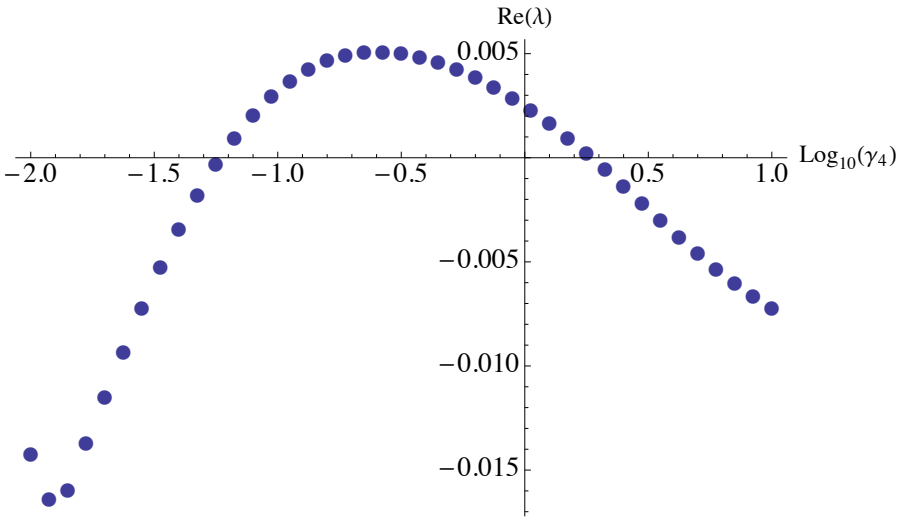


Figure 0.18: **CV2 degradation rate (γ_4) eigenvalue analysis for the equilibrium point exhibiting a Hopf Bifurcation**: The real component of the eigenvalue for the equilibrium point undergoing the Hopf bifurcation as γ_4 is changed. This is the same eigenvalue for variables A, B, M, C, and S. There are two Hopf bifurcations.

0.3.2.5 Time-Delays

Time-delays are important contributors to instability in mathematical models. We have three time delays in this model, τ_1, τ_2, τ_3, representing the transcriptional delays associated with the production of MGP, CV2, and ALK1, respectively, from BMP signaling. Changing the time-delay values does not affect the number of equilibrium points or the equilibrium point concentrations in this model. They only change the stability of the existing equilibrium points. For $\hat{\tau_1}$, a time-delay greater than approximately 1 results in a supercritical Hopf bifurcation (Figure 0.19). The other stable node and unstable node remain unaffected. As $\hat{\tau_1}$ is increased to 40, corresponding to a time delay of 26.67 hours, the equilibrium point remains an unstable spiral and limit cycle dynamics persist.

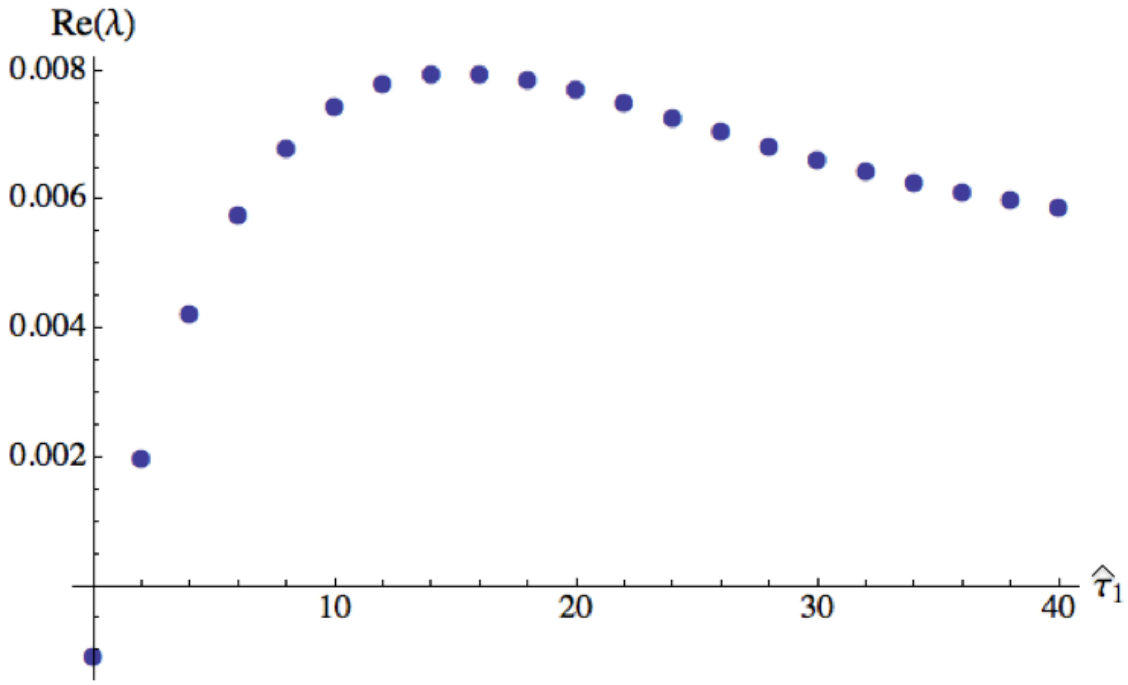


Figure 0.19: τ_1 **eigenvalue analysis for the equilibrium point undergoing a Hopf bifurcation**: The real component of the eigenvalue for the equilibrium point undergoing the Hopf bifurcation as $\hat{\tau}_1$ is changed. This is the same eigenvalue for variables A, B, M, C, and S. $Re(\lambda) > 0$ corresponds to periodic dynamics.

The time delay for CV2 production, τ_2, also exhibits a Hopf bifurcation upon increasing its value. When $\hat{\tau}_2 > 18$, corresponding to a time delay of 12 hrs, the stable spiral equilibrium point becomes an unstable spiral, creating a limit cycle (Figure 0.20). Unlike τ_1, a more substantial time-delay is necessary for τ_2 to initiate periodic dynamics. In vascular endothelial cells, CV2 production exhibits the longest time delay, 20 hrs, compared to MGP and ALK1. The long CV2 time-delay may therefore be necessary for oscillatory gene expression in progenitor HPAECs.

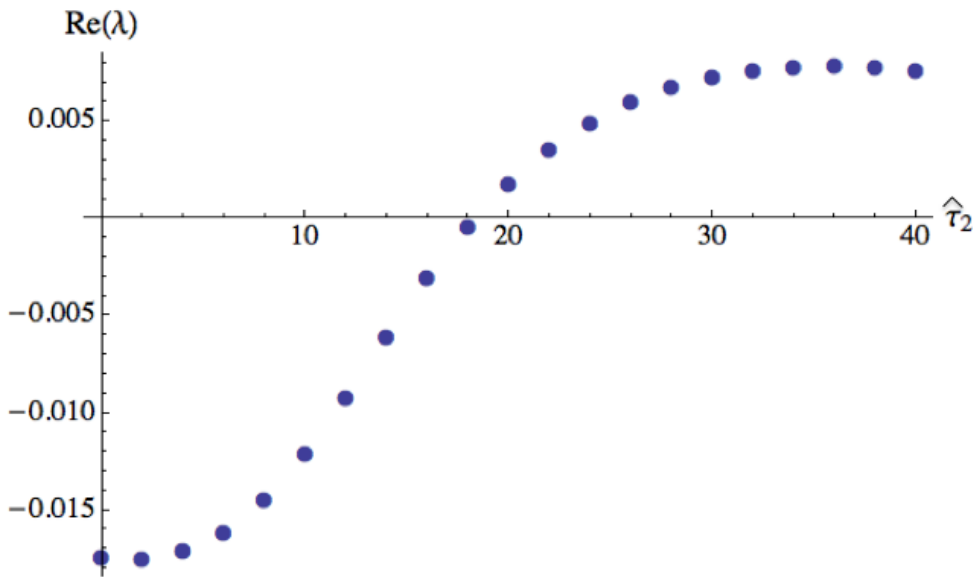


Figure 0.20: τ_2 **eigenvalue analysis for the equilibrium point undergoing a Hopf bifurcation**: The real component of the eigenvalue for the equilibrium point undergoing the Hopf bifurcation as $\hat{\tau_2}$ is changed. This is the same eigenvalue for variables A, B, M, C, and S. $Re(\lambda) > 0$ corresponds to periodic dynamics.

Changes to the final time-delay, τ_3, for BMP-4 induced ALK1 expression also adds instability to the model. When $\hat{\tau_3} < 4$, the system is stable, but past this point the stable spiral node bifurcates into an unstable spiral node causing the system to exhibit limit cycle dynamics (Figure 0.21). The ordered list of time-delays based on the smallest delay required to induce oscillations is τ_1, τ_3, and τ_2, which falls in the same sequence as their biological values. Each experimental time-delay is situated in its respective regime of instability and each is necessary for the existence of oscillations. A summary of the 1-parameter Hopf bifurcation analysis can be found in Table 0.4

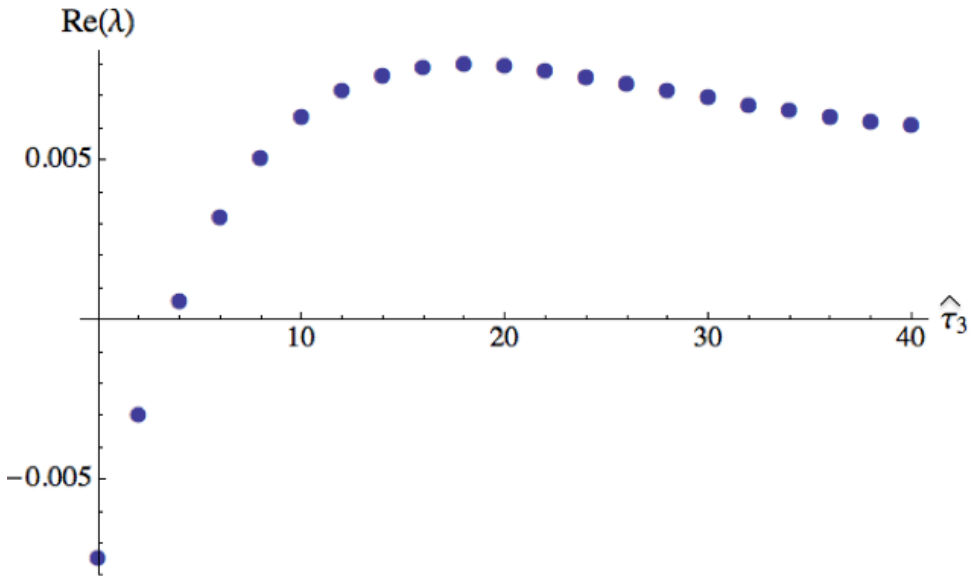


Figure 0.21: τ_3 **eigenvalue analysis for the equilibrium point undergoing a Hopf bifurcation**: The real component of the eigenvalue for the equilibrium point undergoing the Hopf bifurcation as $\hat{\tau}_3$ is changed. This is the same eigenvalue for variables A, B, M, C, and S. $Re(\lambda) > 0$ corresponds to periodic dynamics.

Parameter (p)	Limit Cycle Regime
$log_{10}(\gamma_1)$	[-0.85, -0.20]
$log_{10}(\gamma_2)$	[-1.60, -1.00]
$log_{10}(\gamma_3)$	[-0.15, 0.55]
$log_{10}(\gamma_4)$	[-1.20, 0.20]
$\hat{\tau}_1$	> 1
$\hat{\tau}_2$	>18
$\hat{\tau}_3$	> 4

Table 0.4: **1-Parameter Hopf bifurcation analysis of limit cycle regimes**: the parameter values for which the model exhibits limit cycle dynamics while adjusting the indicated parameter and keeping the rest fixed.

Central take-home points from the 1-parameter Hopf bifurcation analysis:

- Adjusting the γ degradation rates for each variable can lead to a Hopf bifurcation

and limit cycle dynamics.

- γ_1 (BMP-9 degradation) limit cycle region: 7.1 to 1.6 times slower than ALK1 degradation.
- γ_2 (BMP-4 degradatoin) limit cycle region: 40 to 10 times slower than ALK1 degradation
- γ_3 (MGP degradation) limit cycle region: 1.4 times slower to 3.5 times faster than ALK1 degradation.
- γ_4 (CV2 degradation) limit cycle region: 15.8 times slower to 1.6 times faster than ALK1 degradation.
- Oscillations favor the presence of BMP-4 over its antagonist, MGP.
- A slower degradation of BMP-9 compared to BMP-4 helps maintain the negative feedback regulation necessary for oscillations.
- All 3 time-delays are necessary for oscillatory dynamics. CV2 transcription requires a relatively long time delay of 12 hours compared to delays for MGP and ALK1.

0.3.3 2-Parameter Hopf Bifurcation Analysis

Bifurcation analysis on one parameter results in a limited exploration of the parameter space. Varying two parameters simultaneously provides significantly more information about the relationships between the parameters and the stability of the model. We first compare the degradation rates of BMP-4 and BMP-9 for oscillatory behavior.

0.3.3.1 BMP-4 and BMP-9 Degradation

We performed stability analysis on the equilibrium point undergoing a Hopf bifurcation. Figure 0.22 depicts the parameter space between γ_1 and γ_2 that exhibits limit cycle

dynamics. The region of instability for γ_2 is between $[log_{10}(-1.1), log_{10}(-1.7)]$, while γ_1 is contained within $[log_{10}(-0.4), log_{10}(-2.0)]$. This regime is slightly shifted to a higher decay rate of BMP-9 compared to BMP-4.

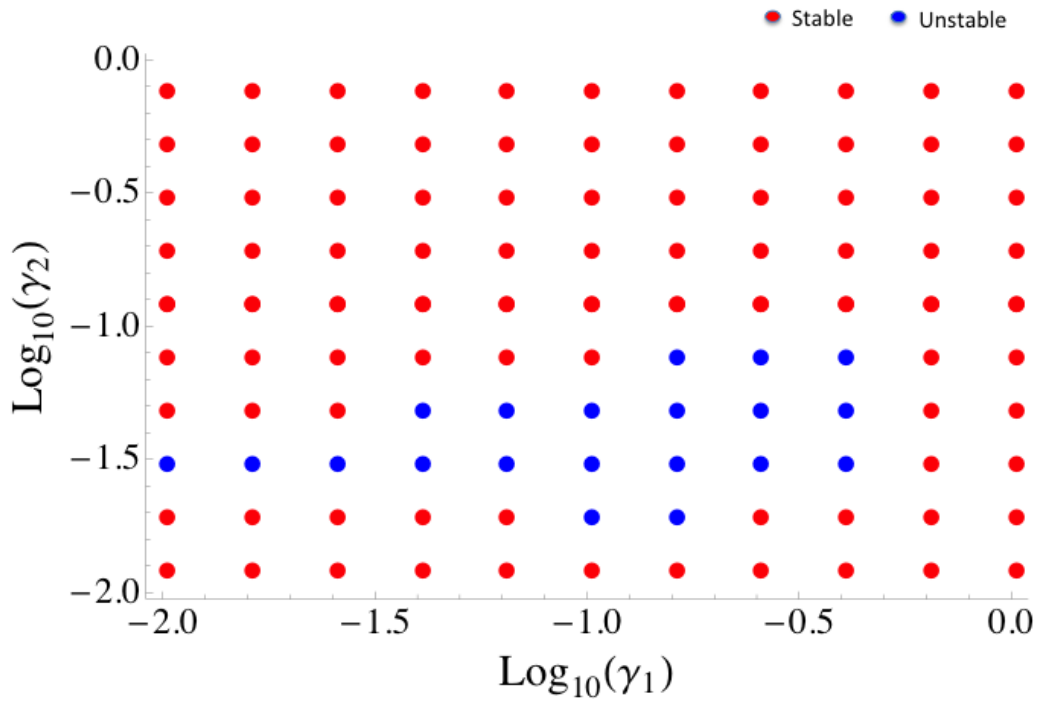


Figure 0.22: **BMP-4 and BMP-9 degradation rate (γ_2, γ_1) stability analysis on the equilibrium point exhibiting a Hopf bifurcation**: γ_1 and γ_2 parameter space analysis for limit cycles. These eigenvalues are the same for the variables A, B, M, C, and S. The red dot marks locations with stable dynamics. The blue dot marks unstable spiral nodes that result in oscillatory kinetics.

0.3.3.2 BMP-4 and MGP Degradation

Next we compared elimination rates of BMP-4 and its inhibitor, MGP. Based on the 1-parameter stability analysis, we predicted that BMP-4 degradation rates should be slower than MGP for the induction of oscillations. The results in Figure 0.23 show that limit cycles exist when γ_2 is between $[log_{10}(-1.7), log_{10}(-1.1)]$ and γ_3 is between $[log_{10}(-1.0), log_{10}(0.6)]$. The degradation rate for MGP must be greater than the rate

for BMP-4 for oscillations to occur. Since the γ parameters are normalized by μ_5, the relative degradation relationship can be interpreted as an absolute one with $\mu_3 > \mu_2$ for the presence of limit cycle dynamics. This supports the hypothesis that the activator, BMP-4, induces oscillations while its antagonist, MGP, suppresses them.

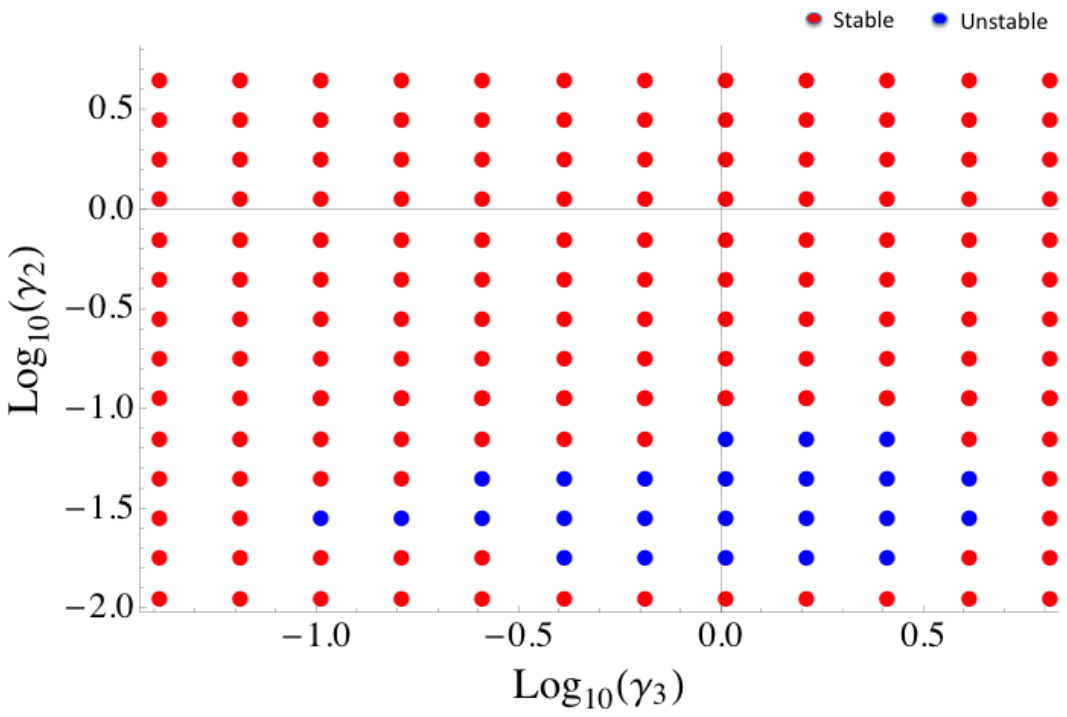


Figure 0.23: **BMP-4 and MGP degradation rate (γ_2, γ_3) stability analysis for the equilibrium point exhibiting a Hopf bifurcation**: γ_1 and γ_3 parameter space analysis for limit cycles. These eigenvalues are the same for the variables A, B, M, C, and S. The red dot marks locations with stable dynamics. The blue dot marks unstable spiral nodes that result in oscillatory kinetics.

0.3.3.3 BMP-4 and CV2 Degradation

We also compared γ_2 to the degradation rate of CV2, γ_4. Once again, the γ_2 parameter space for oscillations is bounded by $[log_{10}(-1.7), log_{10}(-1.1)]$ (Figure 0.24). CV2 degradation, γ_4, has a much larger regime spanning $[log_{10}(-1.0), log_{10}(1.75)]$. BMP-4 degradation consistently has a very specific limit cycle regime corresponding to a

degradation rate that is 50 to 13 times slower than the endocytosis rate of ALK1. CV2 degradation can span a larger region with a degradation rate that is 10 times slower to 56 times faster than the degradation ALK1.

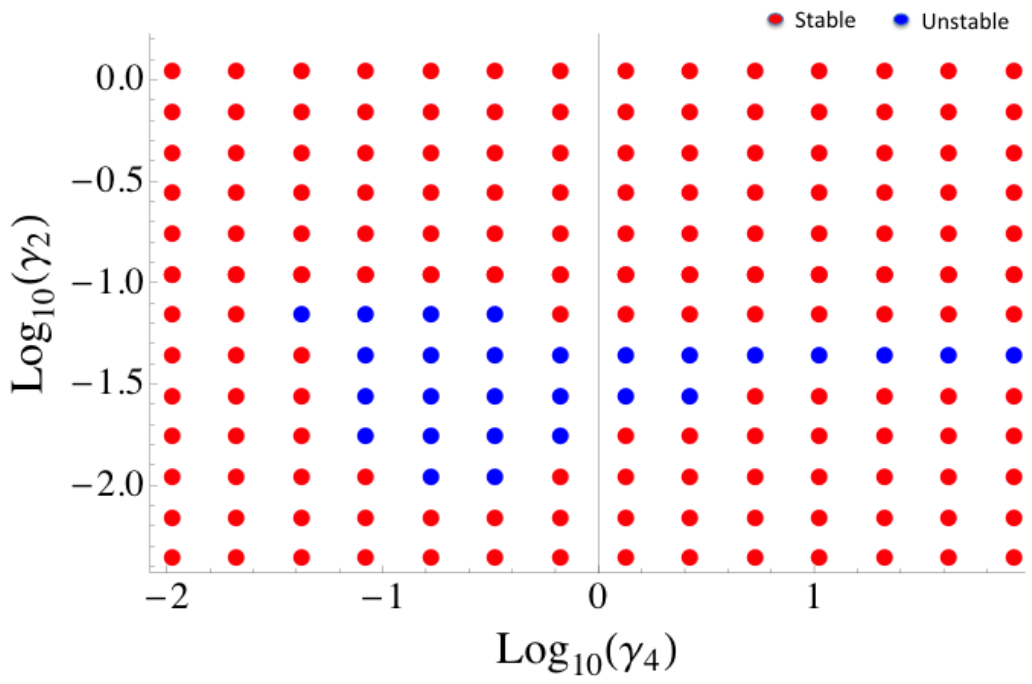


Figure 0.24: **BMP-4 and CV2 degradation rate (γ_2, γ_4) stability analysis for the equilibrium point exhibiting a Hopf bifurcation**: γ_1 and γ_4 parameter space analysis for limit cycles. These eigenvalues are the same for the variables A, B, M, C, and S. The red dot marks locations with stable dynamics. The blue dot marks unstable spiral nodes that result in oscillatory kinetics.

Central take home points from the 2-parameter bifurcation analysis:

- BMP-4 degradation rates that induce oscillations are consistently between 50 to 13 times slower than the degradation rate of ALK1.
- A strictly slower degradation rate of BMP-4 compared to MGP is required for oscillations.

- The presence of BMP-4 is favored over BMP-9 for oscillations.
- CV2 can induce oscillations for a wide range of parameter values, but oscillations tend to favor a greater presence of CV2.

0.4 Experimental Results

The Bostrom Lab conducted experiments measuring mRNA expression of ALK1, MPG, and CV2 after the treatment of progenitor HPAECs with BMP-4 and BMP-9. Initially there is little BMP-4 and BMP-9 in the fetal bovine serum (FBS) that bathes the HPAECs, orders of magnitude less than the initial concentrations added. The addition of 50 ng/ml of BMP-4 to the cell culture results in oscillatory gene expression of ALK1 (Figure 0.25). The oscillations have a period of approximately 24 hours. To determine if BMP-4 is necessary for the oscillations, 100 ng/ml of Noggin and 300 ng/ml of anti-BMP-9 are added to another set of HPAECs. Noggin is a polypeptide the binds to and strongly inhibits BMP-4. Anti-BMP-9 specifically binds to and inhibits BMP-9.

When BMP-4 is inhibited by Noggin, oscillations are eliminated. The mathematical model predicts this finding since the addition of Noggin is analogous to increasing the degradation rate of BMP-4. Thus, the presence of BMP-4 is critical for the oscillatory kinetics of ALK1 seen in the progenitor HPAECs. Both the control group and the BMP-9 treatment group do not demonstrate clear oscillatory behavior, but do result in higher relative ALK1 expression compared to the Noggin + anti-BMP-9 group. This is potentially due to BMP-4 produced by the ECs and BMP-9 in the serum. After approximately 96 hours the cells transition from a pre-confluence to confluence state, that we postulate is associated with further differentiation of progenitor HPAECs to mature HPAECs. The ALK1 mRNA expression oscillates in the pre-confluence phase, but stops once confluence is reached. At the point of confluence there is cell-to-cell contact allowing Delta-Notch signaling to modulate gene expression.

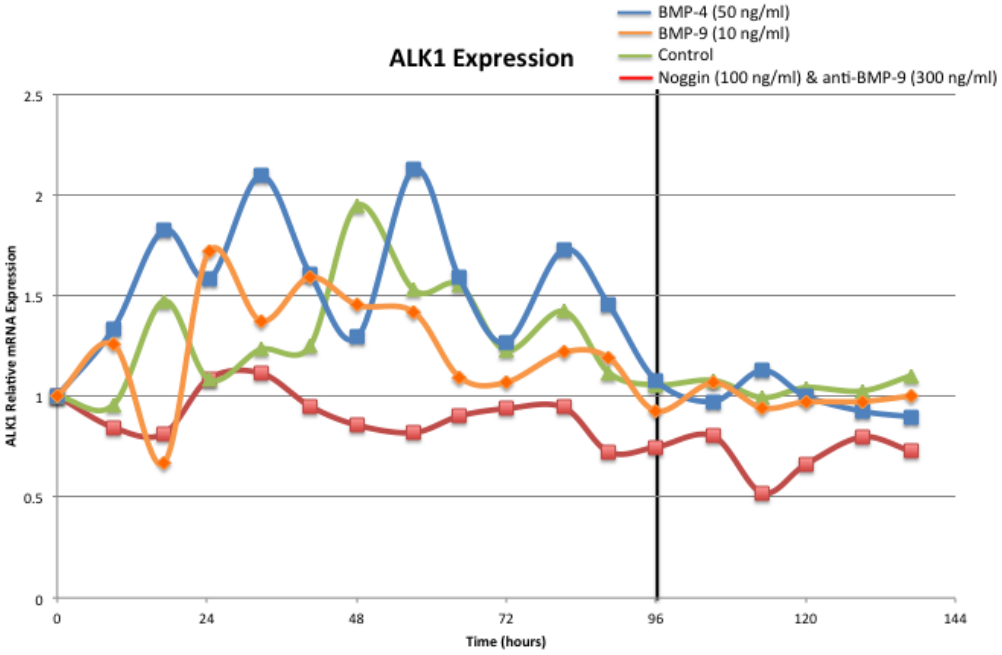


Figure 0.25: **ALK1 relative mRNA expression**: fold change of ALK1 expression after the addition of either BMP-4 (50 ng/ml), BMP-9 (10 ng/ml), Control, or Noggin (100 ng/ml) & anti-BMP-9 (ng/ml) to HPAEC culture. The vertical line marks the approximate point of confluence.

According to the mathematical model, BMP-9 is an essential component to inducing oscillations. Without it, the feedback regulation through MGP and CV2 would not be present thereby eliminating this mechanism for oscillations. Previous modeling of this system by Garfinkel et al. did not include BMP-9 and did not yield oscillatory kinetics [5]. The addition of BMP-9 to the HPAECs lead to an increase in CV2 expression with an approximate time-delay of 20 hours (Figure 0.26). This reflects the significance of including time-delays in the mathematical model. Upon activation, CV2 expression roughly oscillated with a period close to 15 hours. The control group and the addition of BMP-4 are not sufficient to enhance CV2 expression. The addition of anti-BMP-9 and Noggin resulted in reduced CV2 expression without oscillations,

demonstrating the importance of BMP-9 for enhanced periodic CV2 gene expression.

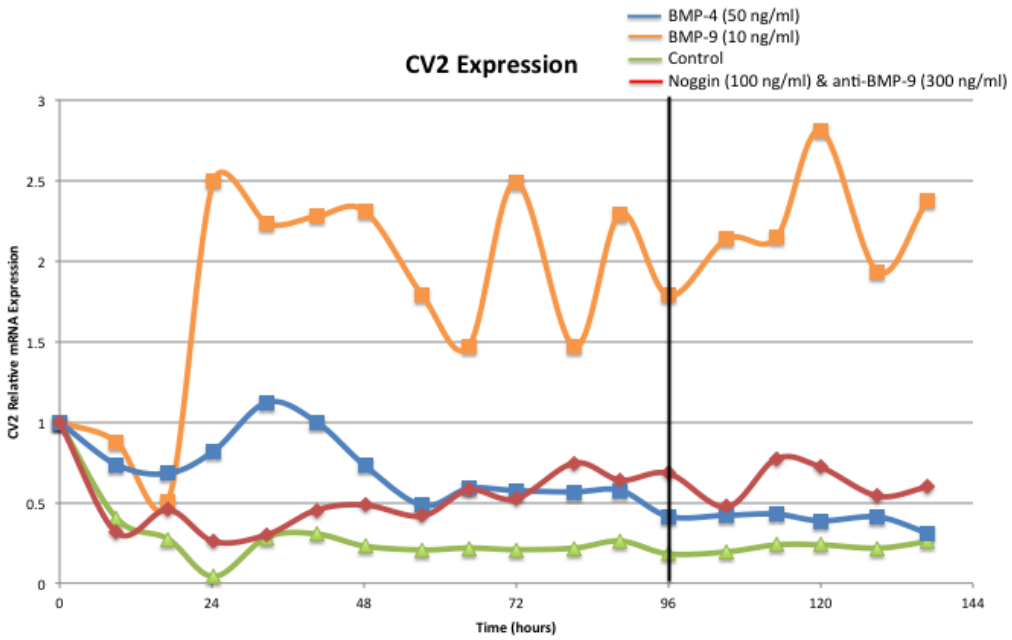


Figure 0.26: **CV2 relative mRNA expression**: fold change of CV2 expression after the addition of either BMP-4 (50 ng/ml), BMP-9 (10 ng/ml), Control, or Noggin (100 ng/ml) & anti-BMP-9 (ng/ml) to HPAEC culture. The vertical line marks the approximate point of confluence.

Furthermore, BMP-9 is essential for MGP expression. The addition of BMP-9 increases MGP expression compared to the control group. The expression oscillates with a period of approximately 24 hours (Figure 0.27). Exogenous BMP-4 cannot induce MGP expression, as expected since BMP-9/ALK1 signaling is responsible for this. The elimination of BMP-9 by anti-BMP-9/Noggin effectively shuts off MGP expression and its oscillatory dynamics.

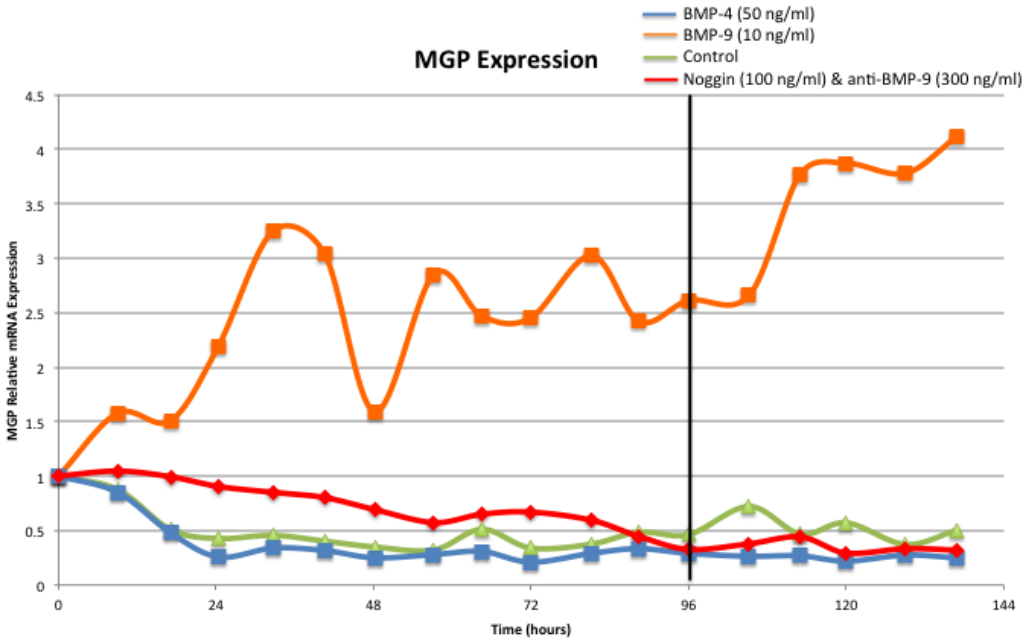


Figure 0.27: **MGP relative mRNA expression**: fold change of CV2 expression after the addition of either BMP-4 (50 ng/ml), BMP-9 (10 ng/ml), Control, or Noggin (100 ng/ml) & anti-BMP-9 (ng/ml) to HPAEC culture. The vertical line marks the approximate point of confluence.

We were also interested in assessing the differentiation state of the HPAECs. We measured the expression of CD34, which is an endothelial progenitor cell marker [26, 41]. In the control group, expression peaked at 3 fold the initial value and steadily declined by day 5 (Figure 0.28). BMP-9 alone did not have an impact on CD34 expression, as expected, since it signals for EC maturation. The initial BMP-4 impulse had the strongest affect on CD34 transcription causing the expression to oscillate and peak at a 5 fold relative increase at day 2.5. CD34 expression declined post-confluence at day 5 to values similar to the other treatment groups. The addition of Noggin reduced CD34 expression and eliminated oscillations. This data supports other scientific findings that BMP-4 is responsible for maintaining the progenitor state, and also provides evidence

that it may do by promoting oscillatory gene expression [26, 41].

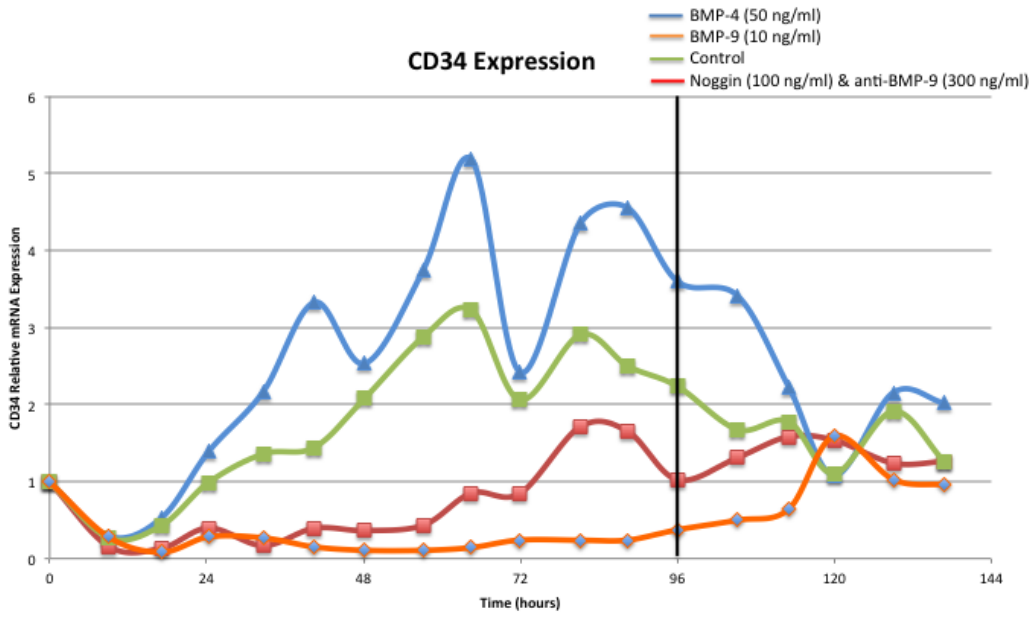


Figure 0.28: **CD34 relative mRNA expression**: fold change of CV2 expression after the addition of either BMP-4 (50 ng/ml), BMP-9 (10 ng/ml), Control, or Noggin (100 ng/ml) & anti-BMP-9 (ng/ml) to HPAEC culture. The vertical line marks the approximate point of confluence.

Ultimately, the process of reaching confluence may play an important role in cell differentiation. In addition to CD34 levels decreasing, there was a rise in MGP expression post-confluence when the culture was induced by BMP-9 (Figure 0.27). The increased MGP likely suppressed BMP-4 activity and possibly inhibited BMP-4 maintenance of the progenitor EC state causing the cells to transition to mature HPAECs.

Central take home points from the experimental results:

- BMP-4 induces oscillations in ALK1 expression in progenitor HPAECs and the inhibition of BMP-4 eliminates them.

- BMP-9 induces oscillations in MGP and CV2 expression in progenitor HPAECs and the inhibition of BMP-4 and BMP-9 eliminates them.
- BMP-4 stimulates oscillations in the expression of the endothelial progenitor marker, CD34, in progenitor HPAECs. BMP-4 may help maintain the HPAEC progenitor state by inducing periodic dynamics.
- Confluence and maturation of the HPAECs appear to eliminate oscillations.
- MGP expression levels exhibit sustained elevation when oscillations are terminated. MGP may play an important role in stopping oscillations and triggering HPAEC maturation.
- ALK1 and CD34 expression levels are reduced upon confluence and maturation.

Connections between the mathematical model and the experimental results:

- The presence of BMP-4 stimulates oscillatory gene expression of ALK1.
- BMP-9, in the presence of BMP-4, stimulates oscillatory gene expression of MGP and CV2.
- Oscillations are terminated by the inhibition of BMP-4 and BMP-9.
- High levels of MGP promote the elimination of oscillations and may function to trigger HPAEC maturation.

0.5 Discussion

In this study, we explored the dynamics of a double-loop negative feedback system containing BMP-4, BMP-9, MGP, and CV2 which are critical for vascular endothelial cell differentiation and morphogenesis [24, 5, 33, 31, 32]. We mathematically studied the mechanisms of oscillatory gene expression in the BMP-4/9 network and the potential role for these oscillations. Only recently have scientists appreciated the significance of oscillatory gene expression in the process of stem cell differentiation [4, 42]. Proteins such as Hes1 exhibit oscillatory dynamics that correspond to different cell fates. Out of phase oscillations between Hes1 and Ngn2 are found in neural progenitor cells, while a transition to sustained expression of high Ngn2 and low Hes1 triggers the cells to differentiate into neural cells [42]. As of now, no one has studied the dynamics of BMP oscillations in progenitor vascular endothelial cells and their potential role in cell differentiation.

We started at first principles, mathematically modeling the activator-inhibitor interactions between BMP-4/MGP and BMP-9/CV2, BMP-4 stimulation of ALK1 expression, and BMP-9/ALK1 signaling of MGP and CV2 expression. This system is known to have long time-delays for the transfer of biological information from ligand-receptor binding to gene expression. Thus, for completeness we modeled the system with 5 nonlinear delay differential equations for BMP-9, BMP-4, MGP, CV2, and ALK1.

Experiments with human embryonic stem cells (hESCs) have shown that BMP-4 Smad- dependent signaling is critical for differentiation into vascular progenitor cells [26]. This progenitor state can further differentiate into mature vascular endothelial cells by BMP-9 signaling [32]. The antagonists, MGP and CV2, work to regulate BMP induced differentiation and maturation by acting on BMP-4 and BMP-9, respectively [43, 32]. We postulate that the negative feedback relationship between BMP-9 and BMP-4 functions as a mechanism to regulate progenitor EC differentiation into mature

ECs, and manifests itself in oscillatory gene expression. This cellular programming can be abstractly thought of as navigating in gene expression state space from an attractor characteristic of progenitor ECs to one that is reflective of mature ECs [3].

We investigated the mathematical model's potential to display oscillatory dynamics using various methods. Non-dimensionalizing the equations significantly reduced the number of parameters in the model and converted them into ratios of dimensional parameters, simplifying the analysis. We approximated all of the parameters except the degradation rates of BMP-9, BMP-4, MGP, and CV2 using experimental values and data from the literature. MC sampling of the parameter space and numerical detection of periodic dynamics in the model helped capture a sense of the parameters inducing oscillatory gene expression. The skewed distribution for γ_2 in the presence of oscillations reflected that BMP-4 elimination should be slower than the rate of ALK1 endocytosis for oscillations to occur.

Linear stability and Hopf bifurcation analysis provided a more detailed view of the model dynamics. In agreement with the MC sampling results, the presence of BMP-4 is critical for oscillations. Also, faster degradation of MGP relative to ALK1 is important for oscillations, highlighting its antagonistic relationship with BMP-4. Oscillations did not occur if BMP-9 was eliminated too quickly due to its role in feedback regulation, and slower degradation of CV2 compared to ALK1 preferentially promoted periodic behavior. The presence of BMP-4 and CV2 induced oscillations while too much MGP inhibited them. If oscillations are interpreted as the progenitor HPAEC state, then BMP-4 and CV2 help maintain the progenitor status of ECs and MGP favors their maturation. This agrees with scientific findings that BMP-4 regulates progenitor status of ECs, and that CV2 antagonizes EC differentiation [26, 32].

While time-delays are often excluded from differential equations due to the added complexity of analyzing the model, they are essential for the production of oscillations in this model under the parameter regime we investigated. The delay for CV2 expression, τ_2, which is 20 hrs in vascular endothelial cells, needed to be greater than

12 hrs in the model for limit cycle dynamics. Therefore, in addition to its negative feedback on BMP-9 and thus MGP expression, CV2 promotes oscillatory dynamics through its long time-delay.

The 2-paramter Hopf bifurcation analyses revealed information about the parameter relationships that are important for periodic dynamics, which could not be obtained from the 1-paramter analyses. BMP-4 degradation rates that exist during oscillations consistently fell in the range of 50 to 13 times slower than ALK1 elimination. Limit cycle dynamics favored relatively slower degradation of BMP-9 compared to ALK1, again demonstrating the need for BMP-9 to be present due to its central role in negative feedback. MGP degradation had to be strictly less than BMP-4 degradation for oscillations to occur, displaying the significance of this activator-inhibitor relationship. This mathematical model predicts that a relatively slow BMP-4 decay rate, coupled with a faster MGP elimination is favored for periodic dynamics.

The experimental findings in the HPAEC culture show agreement with the mathematical model predictions. The addition of BMP-4 induced oscillations in ALK1 expression and the combination of BMP-4 and BMP-9 led to oscillatory MGP and CV2 expression. Treatment of the cell culture with the BMP-4 antagonist, Noggin, and anti-BMP-9 eliminated oscillations and reduced expression of ALK1, MGP, and CV2. The functional role of the oscillations can be postulated by measuring the expression of EC marker, CD34, [41]. BMP-4 increased CD34 expression in an oscillatory manner with a peak increase of 5 fold 2.5 days after being added to the HPAEC culture. Therefore, BMP-4 may help maintain the progenitor EC state through high amplitude oscillations of CD34. This maintenance is eliminated by reduction of BMP-4 levels through Noggin or by the addition of exogenous BMP-9, which functions to promote EC maturation.

Once the cells reached confluence at approximately 96 hours, we believe they differentiated from progenitor to mature HPEACs. This transition is marked by diminished oscillations in ALK1 expression and by the reduced presence of the CD34 progenitor marker. MGP continues to rise after confluence, which may be important

for suppressing oscillations of ALK1 and associated with the maturation of HPAECs. This agrees with findings from the mathematical model that an increased presence of MGP is important for the elimination of oscillations. It may also be connected to the functional role of assisting cell maturation by inhibiting BMP-4 signaling that is critical for maintenance of the progenitor EC state.

Our study is limited due to several factors. The time-delay differential equations do not consider spatial dynamics, including cell-to-cell contact and morphogen diffusion gradients. Thus, it can be interpreted as a pre-confluence model prior to direct cell interactions necessary for Notch signaling. Notch plays an essential role in cell differentiation and pattern formation that we intend to explore in future variations of this model [44, 45]. Furthermore, the BMPs, MGP, and CV2 are diffusible morphogens that are important architects for vascular and pulmonary pattern formation, while ALK1 is a membrane bound receptor [37, 5, 33, 46]. Incorporating spatial dynamics by transforming the equations into delay partial differential equations may provide information about the maturation of progenitor ECs into vascular spatial structures.

Certain pathologies including ateriovenous malformations (AVMs) and diabetic vasculopathies are characterized by increased BMP signaling in endothelial vascular cells [33, 47]. It would be interesting to explore the potential role of the BMP-4/9 regulatory network in pattern formation of pathological angiogenesis and atherosclerotic calcification seen in AVMs and diabetes mellitus, respectively. Deletion of the MGP gene in mice causes AVMs, and hyperglycemia activates aortic BMP activity to promote vascular calcification [47, 31].

AVMs are characterized by reduced capillary branching and the shunting of blood to large-diameter vessels. It would be interesting to explore if temporal oscillations of this system play an important role in spatial vascular patterning, similar to lateral root branching in plants [22]. Preliminary findings from the Bostrom lab indicate that HPAECs form vascular EC networks upon maturation.

In the analysis of this model we made approximations on certain parameters and

focused our methods on exploring the degradation rates of BMP-9, BMP-4, MGP, and CV2 and their affect on equilibrium stability. We intend to explore other parameters in the model, including the production rates and inhibitory coefficients to further study the stability and oscillatory potential of this system. Some experimental limitations in this study included the number of gene expression time-points collected. More time points can help better characterize the oscillations and their properties. Experimentally measuring the expression of BMP-4 will also provide us with a better understanding of the system dynamics, relative to our current limited knowledge of only its experimentally controlled initial conditions.

In summary, our study suggests that a greater presence of BMP-4 relative to its inhibitor, MGP, is important for the induction of oscillatory gene expression. In addition, transcriptional time-delays, such at those for MGP, CV2, and ALK1, play an essential role in adding periodic instability to this system. We also found a possible association between BMP-4 induced oscillatory gene expression and its role in maintaining progenitor HPAECs, as well as, the role of MGP in promoting progenitor differentiation into mature HPAECs. Further experimental studies are necessary to explore this hypothesis.

REFERENCES

[1] M. A. Moreno-Risueno and P. N. Benfey, "Time-based patterning in development: The role of oscillating gene expression," *Transcription*, vol. 2, pp. 124–129, 5 2011.

[2] T. Ohtsuka, M. Ishibashi, G. Gradwohl, S. Nakanishi, F. Guillemot, and R. Kageyama, "Hes1 and hes5 as notch effectors in mammalian neuronal differentiation," *EMBO J*, vol. 18, pp. 2196–207, Apr 1999.

[3] B. D. Macarthur, A. Ma'ayan, and I. R. Lemischka, "Systems biology of stem cell fate and cellular reprogramming," *Nat Rev Mol Cell Biol*, vol. 10, pp. 672–81, Oct 2009.

[4] N. Suzuki, C. Furusawa, and K. Kaneko, "Oscillatory protein expression dynamics endows stem cells with robust differentiation potential," *PLoS One*, vol. 6, no. 11, p. e27232, 2011.

[5] A. Garfinkel, Y. Tintut, D. Petrasek, K. Boström, and L. L. Demer, "Pattern formation by vascular mesenchymal cells," *Proc Natl Acad Sci U S A*, vol. 101, pp. 9247–50, Jun 2004.

[6] M. K. Sinha, J. Sturis, J. Ohannesian, S. Magosin, T. Stephens, M. L. Heiman, K. S. Polonsky, and J. F. Caro, "Ultradian oscillations of leptin secretion in humans," *Biochem Biophys Res Commun*, vol. 228, pp. 733–8, Nov 1996.

[7] R. Refinetti and M. Menaker, "The circadian rhythm of body temperature," *Physiol Behav*, vol. 51, pp. 613–37, Mar 1992.

[8] R. Steinmeier, C. Bauhuf, U. Hübner, R. D. Bauer, R. Fahlbusch, R. Laumer, and I. Bondar, "Slow rhythmic oscillations of blood pressure, intracranial pressure, microcirculation, and cerebral oxygenation. dynamic interrelation and time course in humans," *Stroke*, vol. 27, pp. 2236–43, Dec 1996.

[9] C. J. Goodner, B. C. Walike, D. J. Koerker, J. W. Ensinck, A. C. Brown, E. W. Chideckel, J. Palmer, and L. Kalnasy, "Insulin, glucagon, and glucose exhibit synchronous, sustained oscillations in fasting monkeys," *Science*, vol. 195, pp. 177–9, Jan 1977.

[10] E. W. Kraegen, J. D. Young, E. P. George, and L. Lazarus, "Oscillations in blood glucose and insulin after oral glucose," *Horm Metab Res*, vol. 4, pp. 409–13, Nov 1972.

[11] J. H. McAuley and C. D. Marsden, "Physiological and pathological tremors and rhythmic central motor control," *Brain*, vol. 123 (Pt 8), pp. 1545–67, Aug 2000.

[12] J. N. Weiss, A. Garfinkel, H. S. Karagueuzian, Z. Qu, and P. S. Chen, "Chaos and the transition to ventricular fibrillation: a new approach to antiarrhythmic drug evaluation," *Circulation*, vol. 99, pp. 2819–26, Jun 1999.

[13] S. L. Harris and A. J. Levine, "The p53 pathway: positive and negative feedback loops," *Oncogene*, vol. 24, pp. 2899–908, Apr 2005.

[14] N. A. M. Monk, "Oscillatory expression of hes1, p53, and nf-kappab driven by transcriptional time delays," *Curr Biol*, vol. 13, pp. 1409–13, Aug 2003.

[15] A. Coquelin and C. Desjardins, "Luteinizing hormone and testosterone secretion in young and old male mice," *Am J Physiol*, vol. 243, pp. E257–63, Sep 1982.

[16] B. N. Kholodenko, "Cell-signalling dynamics in time and space," *Nat Rev Mol Cell Biol*, vol. 7, pp. 165–76, Mar 2006.

[17] B. P. Tu, A. Kudlicki, M. Rowicka, and S. L. McKnight, "Logic of the yeast metabolic cycle: temporal compartmentalization of cellular processes," *Science*, vol. 310, pp. 1152–8, Nov 2005.

[18] A. Boiteux, B. Hess, and E. E. Sel'kov, "Creative functions of instability and oscillations in metabolic systems," *Curr Top Cell Regul*, vol. 17, pp. 171–203, 1980.

[19] O. Pourquié, "The segmentation clock: converting embryonic time into spatial pattern," *Science*, vol. 301, pp. 328–30, Jul 2003.

[20] I. Palmeirim, D. Henrique, D. Ish-Horowicz, and O. Pourquié, "Avian hairy gene expression identifies a molecular clock linked to vertebrate segmentation and somitogenesis," *Cell*, vol. 91, pp. 639–48, Nov 1997.

[21] M.-L. Dequéant, E. Glynn, K. Gaudenz, M. Wahl, J. Chen, A. Mushegian, and O. Pourquié, "A complex oscillating network of signaling genes underlies the mouse segmentation clock," *Science*, vol. 314, pp. 1595–8, Dec 2006.

[22] M. A. Moreno-Risueno, J. M. Van Norman, A. Moreno, J. Zhang, S. E. Ahnert, and P. N. Benfey, "Oscillating gene expression determines competence for periodic arabidopsis root branching," *Science*, vol. 329, pp. 1306–11, Sep 2010.

[23] K. Takebayashi, Y. Sasai, Y. Sakai, T. Watanabe, S. Nakanishi, and R. Kageyama, "Structure, chromosomal locus, and promoter analysis of the gene encoding the mouse helix-loop-helix factor hes-1. negative autoregulation through the multiple n box elements," *J Biol Chem*, vol. 269, pp. 5150–6, Feb 1994.

[24] N. L. Boyd, S. K. Dhara, R. Rekaya, E. A. Godbey, K. Hasneen, R. R. Rao, F. D. West, 3rd, B. A. Gerwe, and S. L. Stice, "Bmp4 promotes formation of primitive vascular networks in human embryonic stem cell-derived embryoid bodies," *Exp Biol Med (Maywood)*, vol. 232, pp. 833–43, Jun 2007.

[25] E. S. Shao, L. Lin, Y. Yao, and K. I. Boström, "Expression of vascular endothelial growth factor is coordinately regulated by the activin-like kinase receptors 1 and 5 in endothelial cells," *Blood*, vol. 114, pp. 2197–206, Sep 2009.

[26] H. Bai, Y. Gao, M. Arzigian, D. M. Wojchowski, W.-S. Wu, and Z. Z. Wang, "Bmp4 regulates vascular progenitor development in human embryonic stem cells through a smad-dependent pathway," *J Cell Biochem*, vol. 109, pp. 363–74, Feb 2010.

[27] M. Scharpfenecker, M. van Dinther, Z. Liu, R. L. van Bezooijen, Q. Zhao, L. Pukac, C. W. G. M. Löwik, and P. ten Dijke, "Bmp-9 signals via alk1 and inhibits bfgf-induced endothelial cell proliferation and vegf-stimulated angiogenesis," *J Cell Sci*, vol. 120, pp. 964–72, Mar 2007.

[28] Y. Yao, E. S. Shao, M. Jumabay, A. Shahbazian, S. Ji, and K. I. Boström, "High-density lipoproteins affect endothelial bmp-signaling by modulating expression of the activin-like kinase receptor 1 and 2," *Arterioscler Thromb Vasc Biol*, vol. 28, pp. 2266–74, Dec 2008.

[29] F. S. Govani and C. L. Shovlin, "Hereditary haemorrhagic telangiectasia: a clinical and scientific review," *Eur J Hum Genet*, vol. 17, pp. 860–71, Jul 2009.

[30] D. Umulis, M. B. O'Connor, and S. S. Blair, "The extracellular regulation of bone morphogenetic protein signaling," *Development*, vol. 136, pp. 3715–28, Nov 2009.

[31] Y. Yao, M. Jumabay, A. Wang, and K. I. Boström, "Matrix gla protein deficiency causes arteriovenous malformations in mice," *J Clin Invest*, vol. 121, pp. 2993–3004, Aug 2011.

[32] Y. Yao, M. Jumabay, A. Ly, M. Radparvar, A. H. Wang, R. Abdmaulen, and K. I. Boström, "Crossveinless 2 regulates bone morphogenetic protein 9 in human and mouse vascular endothelium," *Blood*, vol. 119, pp. 5037–47, May 2012.

[33] Y. Yao, S. Nowak, A. Yochelis, A. Garfinkel, and K. I. Boström, "Matrix gla protein, an inhibitory morphogen in pulmonary vascular development," *J Biol Chem*, vol. 282, pp. 30131–42, Oct 2007.

[34] L. David, C. Mallet, M. Keramidas, N. Lamandé, J.-M. Gasc, S. Dupuis-Girod, H. Plauchu, J.-J. Feige, and S. Bailly, "Bone morphogenetic protein-9 is a circulating vascular quiescence factor," *Circ Res*, vol. 102, pp. 914–22, Apr 2008.

[35] A. Schuler-Metz, S. Knöchel, E. Kaufmann, and W. Knöchel, "The homeodomain transcription factor xvent-2 mediates autocatalytic regulation of bmp-4 expression in xenopus embryos," *J Biol Chem*, vol. 275, pp. 34365–74, Nov 2000.

[36] A. Hartung, K. Bitton-Worms, M. M. Rechtman, V. Wenzel, J. H. Boergermann, S. Hassel, Y. I. Henis, and P. Knaus, "Different routes of bone morphogenic protein (bmp) receptor endocytosis influence bmp signaling," *Mol Cell Biol*, vol. 26, pp. 7791–805, Oct 2006.

[37] T.-H. Chen, C. Guo, X. Zhao, Y. Yao, K. I. Boström, M. N. Wong, Y. Tintut, L. L. Demer, C.-M. Ho, and A. Garfinkel, "Patterns of periodic holes created by increased cell motility," *Interface Focus*, vol. 2, pp. 457–64, Aug 2012.

[38] J. D. Murray, *Mathematical Biology: I. An Introduction*, vol. 1. Springer-Verlag, 3 ed., 2002.

[39] T. Erneux, *Applied Differential Equations*, vol. 3. Springer, 2009.

[40] S. H. Strogatz, *Nonlinear Dynamics and Chaos: With Applications to Physics, Biology, Chemistry, and Engineering.* Perseus Books Publishing, 1994.

[41] S.-W. Park, Y. Jun Koh, J. Jeon, Y.-H. Cho, M.-J. Jang, Y. Kang, M.-J. Kim, C. Choi, Y. Sook Cho, H.-M. Chung, G. Y. Koh, and Y.-M. Han, "Efficient differentiation of human pluripotent stem cells into functional cd34+ progenitor cells by combined modulation of the mek/erk and bmp4 signaling pathways," *Blood*, vol. 116, pp. 5762–72, Dec 2010.

[42] H. Shimojo, T. Ohtsuka, and R. Kageyama, "Oscillations in notch signaling regulate maintenance of neural progenitors," *Neuron*, vol. 58, pp. 52–64, Apr 2008.

[43] K. Boström, D. Tsao, S. Shen, Y. Wang, and L. L. Demer, "Matrix gla protein modulates differentiation induced by bone morphogenetic protein-2 in c3h10t1/2 cells," *J Biol Chem*, vol. 276, pp. 14044–52, Apr 2001.

[44] N. D. Lawson, N. Scheer, V. N. Pham, C. H. Kim, A. B. Chitnis, J. A. Campos-Ortega, and B. M. Weinstein, "Notch signaling is required for arterial-venous differentiation during embryonic vascular development," *Development*, vol. 128, pp. 3675–83, Oct 2001.

[45] M. Hellström, L.-K. Phng, J. J. Hofmann, E. Wallgard, L. Coultas, P. Lindblom, J. Alva, A.-K. Nilsson, L. Karlsson, N. Gaiano, K. Yoon, J. Rossant, M. L. Iruela-Arispe, M. Kalén, H. Gerhardt, and C. Betsholtz, "Dll4 signalling through notch1 regulates formation of tip cells during angiogenesis," *Nature*, vol. 445, pp. 776–80, Feb 2007.

[46] Y. Guo, T.-H. Chen, X. Zeng, D. Warburton, K. I. Boström, C.-M. Ho, X. Zhao, and A. Garfinkel, "Branching patterns emerge in a mathematical model of the dynamics of lung development," *J Physiol*, vol. 592, pp. 313–24, Jan 2014.

[47] K. I. Boström, M. Jumabay, A. Matveyenko, S. B. Nicholas, and Y. Yao, "Activation of vascular bone morphogenetic protein signaling in diabetes mellitus," *Circ Res*, vol. 108, pp. 446–57, Feb 2011.